THERMOELECTRIC MATERIAL DEVELOPMENT

FINAL REPORT

Jan W. Vandersande, Camillo Allevato, Thierry Caillat

October 1994

Prepared for

Department of Energy

JPL

Jet Propulsion Laboratory
California Institute of Technology
Pasadena, California

MASTER

DISCLAIMER

Portions of this document may be illegible in electronic image products. Images are produced from the best available original document.

TABLE OF CONTENTS

LIST OF ILLUSTRATIONS

1. Introduction and Background on Skutterudite Materials

In 1981 a search for improved thermoelectric materials at the Jet Propulsion Laboratory was started. The primary objective of this effort was to identify potential candidates for improved thermoelectric performance. The search involved the preparation of the materials, property measurements and modeling of their transport properties. The search has been primarily focused on high temperature materials which could have higher efficiency than state-of-the art SiGe alloys used in Radioisotope Thermoelectric Generators (RTGs). The potential of numerous materials was looked into and the properties of several new compounds were investigated. After the chalcogenides came boron and then several silicides, such as Ru_2Si_3. More recently, a systematic search was started looking for new materials having the following properties:

- Semiconducting properties

- Large Seebeck coefficient

- High carrier mobility

- Low lattice thermal conductivity

- Chemical stability and low vapor pressure

During this search, a new family of materials having the skutterudite structure was identified. Preliminary data obtained on some of the compounds of this family showed that they combine promising electrical and thermal properties [1]. The skutterudite structure was originally attributed to a mineral from Skutterud (Norway) with a general formula (Fe, Co, Ni) As_3 [2]. The skutterudite structure (cubic space group $Im3$, prototype $CoAs_3$) is illustrated in Figure 1. The unit cell contains square radicals $[As_4]^{4-}$. This anion located in the center of the smaller cube is surrounded by 8 Co^{3+} cations. The unit cell was found to consist of 8 smaller cubes (octants) described above but two of them do not have the anions $[As_4]^{4-}$ in the center. This is necessary to keep the ratio Co^{3+}: $[As_4]^{4-}$ = 4:3. Thus, a typical coordination structure results with $Co_8[As_4]_6 = 2$ $Co_4[As_4]_3$ composition and 32 atoms per cell.

A low lattice thermal conductivity and a high carrier mobility are desirable to obtain improved thermoelectric properties in new semiconductor materials. High carrier mobility values are usually found in crystal structures with a high degree of covalency. It has been shown that the bonding is predominantly covalent in the skutterudite structure [3] and high hole mobility values have been measured on several skutterudite compounds: $IrSb_3$ [4], $RhSb_3$ [5] and RhP_3 [6]. The unit cell is relatively large and contains 32 atoms which indicate that low lattice thermal conductivity might be possible. For state-of-the-art thermoelectric materials such as PbTe and Bi_2Te_3 alloys, the number of isostructural compounds is limited and the possibilities to optimize their properties for maximum performance at different temperatures of operation are very limited. This is not the case for the skutterudite family of materials, where ten binary compounds and several solid

solutions and related phases are known to exist. These materials cover a large range of decomposition temperatures and bandgaps which offers the possibility to adjust composition and doping level for a specific temperature range of application. However, very little information is available about their thermoelectric properties and the available data is briefly reviewed in the following sections.

Binary skutterudite compounds are formed with all nine possible combinations of the elements Co, Rh, Ir with P, As, Sb. In this structure each metal atom has six bonds to a pnicogen and each of three pnicogens has two bonds to another pnicogen. Thus, each bond has two electrons which is consistent with the fact that they are diamagnetic semiconductors [7]. Figure 2 shows the room temperature Hall mobility for several p-type binary skutterudite compounds as a function of the Hall carrier concentration. All results were obtained at JPL except for RhP_3 which was found in reference [6]. Values for state-of-the-art semiconductors were also included for comparison. It is clear that the skutterudite compounds have exceptionally high hole mobility, substantially higher than state-of-the-art semiconductors for a given carrier concentration. We have measured a Hall mobility value close to $8000 \, cm^2.V^{-1}.s^{-1}$ on a p-type $RhSb_3$ single crystal with a Hall carrier concentration of about $3.5 \times 10^{18} \, cm^{-3}$. This is the highest p-type mobility ever measured at this doping level and is more than a order of magnitude larger than the best p-type mobilities achieved by state-of-the art thermoelectric materials. All skutterudites have these high hole mobilities which make them very promising materials for thermoelectric applications.

Skutterudite materials offer excellent possibilities to control and optimize the electrical properties by performing suitable substitutions on the transition metal site or the pnicogen site. In natural skutterudite ores, cobalt is often partially replaced by nickel and iron [8]. The substitution limit in the systems $Fe_xCo_{1-x}As_3$ and $Ni_xCo_{1-x}As_3$ has been studied [9]. In the system $Fe_xCo_{1-x}As_3$, with $0 \leq x \leq 0.16$, it was found that the substitution of cobalt by iron decreases the resistivity. For iron concentrations higher than 1%, the conductivity becomes n-type and iron is a donor. The homogeneity limit of the phase $Ni_xCo_{1-x}As_3$ is larger and $0 \leq x \leq 0.65$. Nickel behaves as a donor impurity and the resistivity of the samples decreases with increasing substitution. The conductivity is p-type for $CoAs_3$ and becomes n-type with 1% substitution of nickel for cobalt.

CoP_3 and $CoAs_3$ form a complete range of solid solutions which obey the Vegard's rule [10]. For the system $CoAs_{3-x}Sb_x$ a miscibility gap in the region of $x = 0.4$ to 2.8 was found [10]. These are the only solid solutions between binary skutterudite compounds reported in the literature but it is likely that the other skutterudite compounds form solid solutions, at least in some limited range of composition. Such solid solutions should have lower lattice thermal conductivity than the binary compounds themselves because of the increased point defect scattering. It is also expected that the carrier mobility in these mixed crystals would be lower although they should remain relatively high because of the small difference in electronegativity between the pnicogens, for example, 0.01 (As and P). The ratio between mobility and lattice thermal conductivity would be substantially

5

increased in these mixed crystals, resulting in improved thermoelectric properties. No thermal conductivity measurements of such mixed crystals are available in the literature and the preparation and characterization of samples of various systems would be of great interest. However, we need to know more about the individual binary compounds to estimate their potential temperature range of applications.

The objective of the effort sponsored by DOE was to investigate the potential of n-type skutterudite materials. Because the properties of p-type $IrSb_3$ and $CoSb_3$ were investigated first, efforts concentrated on identifying suitable n-type dopants for these two compounds. Once dopants were identified, the properties of n-type $IrSb_3$ and $CoSb_3$ were investigated and it became clear that solid solutions between these two compounds appeared more promising because the lattice thermal conductivity of the binary compounds was too high, limiting the thermoelectric efficiency. Efforts were then directed to the preparation of n-type solid solutions $IrSb_3$-$CoSb_3$ because significant improvements in the figure of merit by forming solid solutions are possible but only if the relative drop in lattice thermal conductivity is substantially larger than the corresponding decrease in carrier mobility.

The report consists of the following sections:

- Properties of n-type $IrSb_3$ compound
- Properties of n-type $CoSb_3$ compound
- Properties of n-type $IrSb_3$-$CoSb_3$ solid solutions
- Conclusions

2. n-Type IrSb₃ compound

2.1. Methods of Preparation

Previous attempts at growing $IrSb_3$ from Sb-rich melts have always resulted in multiphase samples containing inclusions of Sb. This is due to the peritectic plateau of $IrSb_3$ extending up to 97 at.% Sb [11] and as a consequence only a very narrow range of compositions (with steep temperature variations) is available for crystal growth. Two different techniques were developed for the preparation of polycrystalline $IrSb_3$ samples: hot-pressing of pre-reacted powders (HP) and liquid-solid phase sintering of elemental powders (LSPS). Samples prepared by these methods and with no dopant always showed p-type conductivity. N-type samples have been obtained by adding suitable dopants in elemental form to the mix of Ir and Sb.

2.1.1. Hot-pressing:

The elemental powders (purity of 99.9% or higher) in amounts close to stoichiometric ratios were placed in a glassy carbon crucible, sealed into quartz ampoules under 10^{-5} Torr vacuum and reacted by solid state interdiffusion at 600°C. This temperature has been chosen to prevent the melting of Sb (the element with the lowest melting point, 631°C)

6

and to avoid a segregation phenomenon during synthesis. For mixed Ir and Sb compositions, a reaction time of 24 hours was found sufficient for the synthesis of a completely alloyed powder. This method allowed preparation of large quantities in a relatively contamination-free environment.

The pre-reacted powders were then hot-pressed at 800°C for 2 hours in graphite dies of 6.35 mm ID at pressures of up to 20,000 psi. An "Astro" hot-pressing furnace with a constant flow of argon was used. Compact cylindrical pellets 6.4 mm in diameter and 5 to 8 mm long were obtained by this process. Preparation of the samples by hot-pressing was found to be much more time consuming than the liquid-solid phase sintering approach (LSPS) described in the following section. However, results showed that many HP samples were high quality cylindrical samples with mass densities better than 98% of the theoretical value (using a simple interpolation scheme) before annealing, whereas the LSPS samples were more porous and mass densities were in the 90-94% range of theoretical values.

2.1.2.   Liquid-solid Phase Sintering

Flat bottom 6.35 mm ID quartz ampoules were carbon coated on the inside by cracking acetone and then annealed for a short period of time in vacuum. Elemental powders of Ir and dopants were mixed and placed at the bottom of the ampoules. After, Sb shots were added on top, the ampoules were sealed under vacuum (better than 10^{-5} Torr). Ir and Sb elements were loaded in amounts close to stoichiometric ratios. The ampoules were then heated up to 950°C and held at this temperature for 24 hours. During the process, melted Sb diffused through metal powders and the liquid-solid phase sintering (LSPS) resulted in slightly conical samples about 6.3 mm in diameter and up to 15 mm long.

2.2.   Methods of Physico-Chemical Analysis

Samples were investigated using an optical microscope with and without light polarization or Nomarski contrast to observe their quality and homogeneity. Microprobe analysis (MPA) was performed on selected samples to determine their atomic composition using a JEOL JXA-733 electron superprobe operating at 20 kV of accelerating potential and $25x10^{-9}$ A of probe current. Pure elements were used as standards and X-ray intensity measurements of peak and background were conducted by wavelength dispersive spectrometry. Mass densities were determined using the immersion technique. Because of the substantial porosity found, LSPS samples were held for at least 30 minutes in toluene before weighing to allow the liquid to penetrate the pores. A Siemens D-500 diffractometer produced diffractometry patterns at room temperature. Small additions of Pt or Si powders were made to some samples as an internal standard.

2.3. Measurements of Thermoelectric Properties

The electrical and thermal transport properties of the samples investigated in this program were measured in our different apparatus in the 25-1000°C temperature range. The electrical resistivity and the Hall coefficient were measured by the Van der Pauw method [12] using tungsten probes located on the top surface of the sample as close as possible to the sample's edge (typically a 1 mm thick, 6.35 mm diameter slice). The Seebeck coefficient measurement was conducted by creating a variable temperature difference across the sample and measuring the corresponding linear variation of its thermoelectric voltage [13]. Large samples are usually measured by this technique but samples as thin as 1 mm can also be accommodated. The thermal diffusivity and the heat capacity of selected samples was measured by our flash diffusivity technique [14]. The heat capacity determination is a delicate measurement, but provided a careful calibration of the system (heat input from the flash lamp) is conducted on a standard graphite sample, we have found that reasonably good data can be obtained.

2.4. Thermoelectric Properties

Samples prepared with no dopant always showed p-type conductivity and numerous dopants have been experimentally investigated in order to produce n-type $IrSb_3$. Samples doped with Pt, Ni, Pd, Ag, Te, Se, Au, Cu, I, Re, Bi, Pb, Yb, Ge, Sm, Ga, Mn, Zn, B, Al, In and Hg were prepared. Dopants concentration were ranging between 0.1 and 0.15 at.%. Samples doped with Ni, Pd, Ag, Te, Se, Au, Cu, I, Re, Bi, Pb Yb, Ge, Sm, Ga, Mn, Zn, B, Al and Hg all have p-type conductivity.

Only Pt was found to be a good n-type dopant in $IrSb_3$. Doping with Pt concentration between 0.05 and 0.15 at.% changed the conductivity to n-type. MPA of the samples doped with Pt concentrations higher than 0.15 at.% always showed some secondary phases and the solubility limit of Pt in $IrSb_3$ is about 0.15 at.%.

Room temperature van der Pauw, Hall coefficient, Hall carrier concentration and Seebeck coefficient measurements of Pt doped $IrSb_3$ samples are summarized in Table 1.

Table 1: Room temperature thermoelectric properties of single phase homogeneous selected n-type $IrSb_3$ samples prepared by LSPS and doped with Pt

Sample #	Nominal dopant (at.%)	ρ (mΩ.cm)	n/p (x10^{19} cm^{-3})	μ_H (cm^2.V^{-1}.s^{-1})	α (μV.K^{-1})
2IS50	0.15 Pt	8.36	3.3	-24	-120
3IS52	0.13 Pt	14.39	1.29	-34	-275
4IS32	0.1 Pt	70.3	0.126	-72	-502
1IS35	0.05 Pt	854	0.072	-10	-345

N-type samples have higher electrical resistivity than p-type samples [15] because n-type mobilities are substantially lower than p-type. N-type Seebeck coefficients are larger than p-type Seebeck coefficients [15] which indicates a difference in the hole and electron effective masses. An estimate of the effective masses can be made from the room temperature values of the Hall carrier concentration and Seebeck coefficient as follows. The Seebeck coefficient (α) can be expressed using generalized Fermi-Dirac statistics formalism and assuming acoustic phonon scattering of the charge carriers:

$$\alpha = \pm \frac{k}{e} \left(2 \frac{F_1(\xi)}{F_0(\xi)} - \xi \right) \qquad (1)$$

where k is the Boltzmann constant, e the electron charge, ξ the Fermi level, and F_1 and F_0 are Fermi integrals. Using the same formalism, the Hall carrier concentration (n/p) can be expressed as:

$$n/p = 4/\sqrt{p} \ (2\pi m^* kT/ h^2)^{3/2} \ F_{1/2} \ (\xi) \qquad (2)$$

Using the room temperature values of the Seebeck coefficient and assuming acoustic phonon scattering, the Fermi level ξ can be calculated from equation (1) and used in equation (2) to calculate the effective mass m^*. Using the data tabulated in Table I, an average mass $1.51 \ m_o$ was calculated for the electrons. This mass is rather large compared to the hole mass which was estimated at $0.17 \ m_o$ [15] and explains the large values of the n-type Seebeck coefficients.

High temperature measurements were conducted on selected samples and the results are reported in Figures 3, 4 ,5 and 6 for the electrical resistivity, Hall mobility, Seebeck coefficient and thermal conductivity, respectively. Figure 3 shows the electrical resistivity value as a function of the temperature for several n-type samples with different doping levels. These samples clearly show an intrinsic behavior at high temperatures and a bandgap of 1.18 eV was estimated from the linear variations of the electrical resistivity at high temperatures. The variations of the Hall mobility are shown in Figure 4. The Hall mobility of the samples is n-type up to about 300°C and becomes p-type for higher temperatures, increasing up to about 700°C. This due to compensation effects by high mobility holes. The high temperature Seebeck coefficient values are shown in Figure 5. For lightly doped n-type samples, minority carrier compensation effects are also observed and the Seebeck coefficient changes sign at relatively low temperatures, becomes positive and then follows the variations of typical p-type samples at high temperatures [15]. For n-type samples with a high doping level, the Seebeck coefficient remains n-type up to a temperature of about 700°C.

The thermal conductivity of two n-type samples was calculated from thermal diffusivity and heat capacity measurements up to 700°C and the results are shown in Figure 6. The thermal conductivity decreases from a room temperature of about 95 $mW.cm^{-1}.K^{-1}$ to a minimum value of about 35 $mW.cm^{-1}.K^{-1}$ at a temperature of 650°C. The lattice thermal conductivity was estimated by substracting the calculated electronic contribution to the total thermal conductivity using Wiedeman-Franz law and was found to represent 90% of the total thermal conductivity: 85 $mW.cm^{-1}.K^{-1}$. Figure 7 shows the calculated ZT values for two n-type samples doped with Pt. ZT values increase with temperature, reach a maximum of about 0.16 at a temperature of 500°C and then decrease with increasing temperature corresponding to the decrease of the Seebeck coefficient above this temperature for heavily doped n-type samples. Relatively low ZT were obtained for n-type $IrSb_3$ mainly because the lattice thermal conductivity of $IrSb_3$ is too large. Reduction of the lattice thermal conductivity can be achieved by forming solid solutions between isostructural compounds. $CoSb_3$ is isostuctural to $IrSb_3$ and the properties of p-type $IrSb_3$-$CoSb_3$ were investigated in parallel to this effort on n-type skutterudite materials. Before investigating the properties of the solid solutions, the properties of n-type $CoSb_3$ were characterized and are presented in the following section.

3. n-Type $CoSb_3$ compound

3.1.   Methods of Preparation and Physico-Chemical Analysis

The Co-Sb phase diagram shows that the growth of the compound $CoSb_3$ can be initiated from Sb rich melts between 91 and ~ 97 at.% Sb [16]. Crystals of $CoSb_3$ were grown using the gradient freeze technique from melts with 93 at.% Sb in sealed quartz ampoules coated with carbon. A temperature gradient of about 50°C/cm was maintained at the growth interface and the growth rate was about 0.7°C/hour. Dopants were added to the original melts to produce n-type conductivity samples. Typical ingots after the growth were composed of two parts: the bottom part corresponding to the compound $CoSb_3$ and the upper part corresponding to the Sb-rich eutectic. The crystals were investigated using the techniques described in section 2.2. Selected samples were polished and their microstructure was investigated under an optical microscope. Some samples were ground for X-ray diffractometry (XRD) analysis. The results showed that the samples were single phase and the obtained patterns corresponded to the skutterudite structure. Density of the samples were measured and were found to be about 99.5% of the theoretical density (7.69 $g.cm^{-3}$). Samples were cut from the ingots in the form of disks about 2 mm thick and 10 mm in diameter. The thermoelectric properties of these samples were measured using the techniques described in section 2.3. and are presented in the following section.

3.2.   Thermoelectric Properties

Te was found to be a good n-type dopant for $CoSb_3$ and samples with n-type conductivity were obtained by doping with Te concentrations between 0.08 and 0.15 at.%. Room temperature van der Pauw, Hall effect and Seebeck coefficient are

summarized in Table 2. N-type samples cut from the same ingot have different carrier concentration because of the segregation of Te during the directional crystallization.

Table 2:   Room temperature thermoelectric properties of single phase homogeneous selected n-type CoSb$_3$ crystals prepared by LSPS and doped with Te

Sample #	Nominal dopant (at.%)	ρ (mΩ.cm)	n/p (x10^{19} cm^{-3})	μ_H (cm^2.V^{-1}.s^{-1})	α (μV.K^{-1})
1CS10	0.08 Te	14.2	0.454	-101.0	-500
3CS10	0.08 Te	7.627	0.969	-84.4	-380
1CS7	0.1 Te	11.64	0.494	-108.8	-450
2CS9	0.12 Te	5.99	1.520	-68.0	-270
2CS9A	0.12 Te	9.2	0.920	-70.0	-410
1CS11	0.15 Te	5.572	1.287	-87.0	-373

N-type samples have higher electrical resistivity than p-type samples [17] because n-type Hall mobilities are substantially lower than p-type. Similarly to n-type IrSb$_3$, n-type CoSb$_3$ samples have large Seebeck coefficient and using the same formalism described in section 2.4., the electron effective mass was estimated at 1.65 m$_0$ for CoSb$_3$. The electron effective mass is relatively large for CoSb$_3$ and explains the relatively large Seebeck coefficient values measured on the n-type samples. The band structure seems to be very similar for CoSb$_3$ and IrSb$_3$ because the hole and electron effective masses have very close values in both compounds.

High temperature measurements were conducted on selected samples and are shown in Figures 8, 9, 10, 11 for the electrical resistivity, Hall mobility, Seebeck coefficient and thermal conductivity, respectively. Figure 8 shows the high temperature values of the electrical resistivity for several n-type Te doped samples with different doping levels. For all the samples the electrical resistivity increases with increasing temperature up to a temperature of about 250°C. Above this temperature the variations of the electrical resistivity are linear with temperature with an activation energy of about 0.55 eV. Figures 9 and 10 show the variations of the Hall mobility and Seebeck coefficient as a function of temperature for n-type CoSb$_3$ samples doped with Te. The Hall mobility is negative up to about 200°C and becomes positive for higher temperature where the minority carrier (holes) conduction becomes more significant. The Hall mobility increases up to about 400°C and then decreases up to 550°C. The variations of the Seebeck coefficient are quantitatively similar to the variations of the Hall mobility. However, the Seebeck coefficient changes sign at about 300°C, higher than for the Hall mobility.

The thermal conductivity of two n-type samples was measured up to about 500°C and the values are shown in Figure 11. The values for one p-type sample is also shown for comparison [17]. The thermal conductivity decreases from room temperature up to

about 400°C, reaches a minimum value of about 40 mW.cm^{-1}.K^{-1} and then increases due to increasing minority carrier conduction (bipolar contribution). The lattice thermal conductivity was estimated by substracting the calculated electronic contribution to the total thermal conductivity and was found to be about 90% of the total thermal conductivity: 103 mW.cm^{-1}.K^{-1}. Figure 12 shows the calculated ZT of one n-type CoSb$_3$ sample. ZT reaches a maximum of 0.05 at about 150°C and then decreases with increasing temperature. At about 350°C, the sample changes from n-type to p-type and the ZT values increase up to about 450°C and decrease for higher temperatures. Although no efforts were made to optimize the doping level, ZT values seem to be limited by the relatively large thermal conductivity values as for IrSb$_3$.

ZT values of n-type samples of the compounds CoSb$_3$ and IrSb$_3$ are limited by the relatively large thermal conductivity of these compounds. Lowering the lattice thermal conductivity can be obtained for solid solutions where point defect phonon scattering is increased. We applied this approach to the system Co$_x$Ir$_{1-x}$Sb$_3$ and investigated the properties of n-type solid solutions in this system.

4. n-Type CoSb$_3$-IrSb$_3$ Solid Solutions

4.1. Methods of Preparation and Physico-Chemical Analysis

No quasibinary alloying behavior was expected due to the incongruent melting character of the compounds (peritectic decomposition temperature of 1141°C for IrSb$_3$ and 929°C for CoSb$_3$). Also the difference in lattice parameter values between the two binary compounds is substantial, about 2.3%. However, MPA and X-ray analysis demonstrated that a partial solid solution range exist between the IrSb$_3$ and CoSb$_3$ compounds [18]. In the system Co$_x$Ir$_{1-x}$Sb$_3$, there is a miscibility gap for 0.2<x<0.65. Samples were prepared exclusively using the LSPS technique described in section 2.1.2. with the following adaptations. Elemental powders of Ir, Co and one dopant were loaded at the bottom of the ampoules and Sb shots were then added at the top. Co, Ir, Sb and dopant were loaded in amounts close to stoichiometric ratios. The ampoules were then heated up to 800°C for Co-rich solid solutions and up to 950°C for Ir-rich solid solutions. The temperature was held for 24 hours. Samples about 6.3 mm in diameter and about 15 mm long were produced.

The properties of three different solid solutions in the system Co$_x$Ir$_{1-x}$Sb$_3$ were investigated. For the Ir-rich solid solution (Co$_{0.12}$Ir$_{0.88}$Sb$_3$), Pt was used as a dopant because it was found to be a good dopant for IrSb$_3$. Samples of two Co-rich solid solutions were also prepared. For the solid solution Co$_{0.94}$Ir$_{0.06}$Sb$_3$, Te and Pt were used as dopants and for the solid solution Co$_{0.88}$Ir$_{0.12}$Sb$_3$, Te, Pt, Tl and In were used.

4.2. Thermoelectric Properties

4.2.1. Room Temperature Properties

The room temperature properties of some Pt doped, single phase and homogeneous samples of the solid solution $Co_{0.12}Ir_{0.88}Sb_3$ are reported in Table 3.

Table 3: Room temperature properties of single phase homogeneous selected n-type $Co_{0.12}Ir_{0.88}Sb_3$ solid solutions prepared by LSPS and doped with Pt

sample	nominal concentration of platinum (at.%)	d	ρ	μH	n	α	PF (α²/ρ)
1DD332	.12 Pt	8.624	81.4	0.7	10.50	101.3	0.1
2DD332	.12 Pt	8.515	43.8	3.8	3.79	159.1	0.6
3DD332	.12 Pt	8.586	39.0	3.4	4.77	162.0	0.7
1KD326	.2 Pt	8.219	13.2	0.1	329.0	249.8	4.7
2KD326	.2 Pt	8.107	11.6	0.2	25.30	175.0	2.6
3KD326	.2 Pt	7.584	19.6	3.8	8.48	145.7	1.1
4KD326	.2 Pt	7.524	18.1	3.5	9.95	171.5	1.6
1DD331	.6 Pt	8.446	8.3	3.2	23.60	131.5	2.1
2DD331	.6 Pt	8.366	7.6	3.9	21.0	104.9	1.5
3DD331	.6 Pt	8.256	8.0	3.9	19.80	119.5	1.8

(d) density ($g.cm^{-3}$), ρ electrical resistivity ($m\Omega.cm$), (μH) Hall mobility ($cm^2.V^{-1}s^{-1}$), (α) Seebeck coefficient ($\mu V.K^{-1}$) and PF power factor ($\mu W.cm^{-1}K^{-2}$)

The samples were doped with Pt concentration between 0.12 and 0.6 at%. The solubility limit of Pt seems to be higher in this solid solution than in $IrSb_3$. With increasing Pt concentration in the samples, their electrical resistivity decrease and a minimum value of 7.6 $m\Omega.cm$ was achieved. The room temperature properties of some Pt and Te doped, single phase and homogeneous samples of the solid solution $Co_{0.94}Ir_{0.06}Sb_3$ are reported in Table 4. Doping with Te or Pt concentration of 0.2 at% produced n-type samples. Finally, the room temperature properties of some Pt, In, Tl and Te doped, single phase and homogeneous samples of the solid solution $Co_{0.88}Ir_{0.12}Sb_3$ are reported in Table 5. Samples containing In, Tl, Te and Pt concentration between 0.2 and 0.6 at% have n-type conductivity.

Table 4: Room temperature properties of single phase homogeneous
selected n-type $Co_{0.94}Ir_{0.06}Sb_3$ solid solutions prepared by LSPS and
doped with Pt or Te

sample	nominal concentration of dopant (at.%)	d	ρ	μ_H	n	α	PF (α^2/ρ)
1DD344	.2Pt	6.860	2.6	44.6	5.39	238.9	22.0
2DD344	.2Pt	6.880	2.8	53.8	4.17	266.0	25.5
MDD344	.2Pt	6.650	3.2	35.0	5.50	221.2	15.1
3DD344	.2Pt	6.740	3.7	23.2	7.18	194.7	10.2
4DD344	.2Pt	6.510	4.2	18.0	8.33	225.6	12.2
1DD345	.2Te	6.979	3.3	69.9	2.68	319.6	30.7
2DD345	.2Te	7.040	3.9	75.3	2.08	313.9	25.4
3DD345	.2Te	6.790	6.4	49.5	1.99	269.5	11.4
4DD345	.2Te	6.700	7.3	29.0	2.96	323.5	14.4

(d) density (g.cm^{-3}), ρ electrical resistivity (mΩ.cm), (μH) Hall mobility (cm^2.V^{-1}s^{-1}), (α) Seebeck coefficient (μV.K^{-1}) and PF power factor (μW.cm^{-1}K^{-2})

Doping with Te or Pt concentration of 0.2 at% produced n-type samples. Finally, the room temperature properties of some Pt, In, Tl and Te doped, single phase and homogeneous samples of the solid solution $Co_{0.88}Ir_{0.12}Sb_3$ are reported in Table 5. Samples containing In, Tl, Te and Pt concentration between 0.2 and 0.6 at% have n-type conductivity.

In order to assess the impact of the solid solution formation on the electrical properties of n-type samples, a comparison of the Hall mobility of the samples for the binary compounds and the solid solutions was done and is represented in Figure 13. For the same carrier concentration, the Hall mobility of n-type CoSb$_3$ samples is significantly higher than the Hall mobility of n-type IrSb$_3$. For the solid solutions, the same trend is observed. Hall mobilities measured on samples of the Ir-rich solid solution are significantly lower than those for the Co-rich solid solutions. A maximum Hall mobility value of 3.9 cm^2.V^{-1}.s^{-1} was measured for the Ir-rich solid solution and a maximum value of about 75 cm^2.V^{-1}.s^{-1} was measured for the Co-rich solid solutions. In solid solutions, it is expected to observe a decrease in the Hall mobility due to an increase of the carrier scattering rate because of the mass disorder. However, it seems that different scattering mechanisms are present in Co and Ir-rich solid solutions, resulting in a significant decrease in the Hall mobility for the Ir-rich solid solution while the Hall mobility in Co-rich solid solutions is less reduced.

Table 5: Room temperature properties of single phase homogeneous selected n-type $Co_{0.88}Ir_{0.12}Sb_3$ solid solutions prepared by LSPS and doped with Pt, In, Tl or Te

sample	nominal concentration of dopant (at.%)	d	ρ	μ_H	n	α	PF (α^2/ρ)
1DD336	.2 In	7.110	180	53.0	0.07	606.0	2.0
2DD336	.2 In	6.970	234	33.0	0.08	490.0	1.0
1DD328	.6 In	6.660	3.5	49.8	3.55	254.0	18.3
2DD328	.6 In	6.567	3.7	50.7	3.35	236.7	15.2
3DD328	.6 In	6.220	4.4	36.3	3.87	215.0	10.4
4DD328	.6 In	6.102	4.8	35.9	3.62	260.0	14.0
1DD329	.2 Pt	7.053	2.8	62.7	3.59	246.0	21.8
2DD329	.2 Pt	6.828	3.7	47.0	3.54	395.0	41.6
3DD329	.2 Pt	7.300	2.4	47.2	5.57	234.0	23.1
4DD329	.2 Pt	7.216	2.1	37.7	7.99	222.0	23.8
1DD337	.2 Pt	7.050	5.3	73.0	1.60	347.0	22.8
2DD337	.2 Pt	6.889	5.2	54.9	2.17	402.0	30.9
3DD337	.2 Pt	6.970	2.5	55.0	4.61	220.0	19.7
4DD337	.2 Pt	6.900	3.5	57.9	3.08	337.0	32.5
1DD342	.2Pt	6.969	3.0	62.6	3.37	249.0	21.0
2DD342	.2Pt	7.050	2.9	56.2	3.79	281.0	27.0
3DD342	.2Pt	7.130	4.0	42.3	3.74	218.0	12.0
4DD342	.2Pt	7.090	5.5	23.6	4.77	210.4	8.0
1DD338	.2 Te	6.960	3.6	58.9	2.96	320.0	28.7
2DD338	.2 Te	6.880	3.5	62.0	2.87	325.0	30.2
3DD338	.2 Te	6.530	8.5	25.2	2.92	305.0	11.0
4DD338	.2 Te	6.560	10.0	23.2	2.67	316.0	10.0
1DD343	.2Te	6.970	3.8	53.2	3.07	329.8	28.5
2DD343	.2Te	6.878	3.6	62.9	2.74	342.8	32.5
MDD343	.2Te	6.799	4.5	44.1	3.11	221.6	10.8
3DD343	.2Te	6.815	8.5	34.4	2.14	302.2	10.8
4DD343	.2Te	6.975	8.9	26.0	2.70	253.9	7.2
2DDT4	.2 Tl	6.960	4.0	52.5	3.00	319.0	25.7
3DDT4	.2 Tl	6.710	5.7	51.8	2.12	346.0	21.1
4DDT4	.2 Tl	6.980	9.7	34.2	1.89	325.0	10.9

(d) density ($g.cm^{-3}$), ρ electrical resistivity ($m\Omega.cm$), (μH) Hall mobility ($cm^2.V^{-1}s^{-1}$), (α) Seebeck coefficient ($\mu V.K^{-1}$) and PF power factor ($\mu W.cm^{-1}K^{-2}$)

The electrical resistivity values of $CoSb_3$, $IrSb_3$, Co and Ir-rich solid solutions samples are shown in Figure 14. Because the Hall mobility of the Ir-rich samples are much lower than those for the Co-rich, the electrical resistivity of the samples of the Ir-rich solid

15

solution are significantly larger than those of the Co-rich solid solutions. A minimum electrical resistivity value of 7.6 mΩ.cm was measured for the Ir-rich solid solution and a minimum value of about 2 mΩ.cm was measured for the Co- solid solutions. For carrier concentration above 10^{20}cm^{-3}, the electrical resistivity of the samples are higher. These samples are likely to be compensated at room temperature (mixed conduction) and the Hall carrier concentration measured on these samples does not correspond to an extrinsic carrier concentration.

The Seebeck coefficient values for CoSb$_3$, IrSb$_3$, Co and Ir-rich solid solutions samples are shown in Figure 15 as a function of the carrier concentration. In a solid solution system, it is not expected to observe significant changes in the Seebeck coefficient with composition and at a similar doping level unless the binary compounds have significantly different band structure which is not the case in this system. The electron effective mass value of CoSb$_3$ and IrSb$_3$ are similar and consequently the Seebeck coefficient values for a given carrier concentration are similar for CoSb$_3$, IrSb$_3$, Co and Ir-rich solid solutions samples.

Figure 16 shows the room temperature power factor values (α^2/ρ) as a function of temperature for Co and Ir-rich solid solution samples. The values for the Ir-rich solid solution samples are low and do not exceed 3 μW.cm^{-1}K^{-2}. For Co-rich solid solutions the power factor values are significantly larger and the maximum value is about 30 μW.cm^{-1}K^{-2} for a carrier concentration of about 3 x 10^{19}cm^{-3}. Figure 16 clearly shows that the optimum carrier concentration range is between 2 and 4 x 10^{19}cm^{-3}. The high temperature properties of several samples with the highest room temperature power factor were measured and the results are presented in the next section.

4.2.2. High Temperature Properties

Figure 17 shows the high temperature values of the electrical resistivity as a function of inverse temperature for several samples of Co and Ir-rich solid solutions. For all Co-rich solid solution samples, the electrical resistivity increases with increasing temperature up to about 400°C and then decreases due to increasing minority carrier (holes) conduction. For the Ir-rich solid solution samples, the resistivity is higher and increases only very slightly with temperature and decreases at high temperatures also due to increasing minority carrier concentration. At high temperature, the electrical resistivity varies almost linearly with inverse temperature and the activation energy is clearly higher for the Ir-rich solid solution sample than for Co-rich solid solution samples. This is expected because the bandgaps of CoSb$_3$ and IrSb$_3$ were estimated at 0.55 and 1.18 eV, respectively.

Figure 18 shows the high temperature values of the Hall mobility as a function of temperature for n-type Co and Ir-rich solid solution samples. The Hall mobility is negative up to about 300°C and then becomes positive when hole conduction increases. The experimental Seebeck coefficient values are shown in Figure 19 as a function of temperature. The Seebeck coefficient for all Co-rich solid solution samples is large at low

16

temperature and nearly constant up to about 300°C where it starts decreasing because of increasing minority carrier conduction similarly to the variations of the Hall mobility. The intrinsic behavior becomes more important at higher temperature and the Seebeck coefficient of the samples decreases sharply. The Seebeck coefficient of the Ir-rich sample is much lower but this is likely due to some compensation effects which are already observed at room temperature. Combining the measurements of the electrical resistivity and Seebeck coefficient, the power factor values for Co and Ir-rich solid solution samples are shown in Figure 20 as function of temperature. Again, because the electrical resistivity of Ir-rich solid solution samples is larger than those for Co-rich, the power factor of Ir-rich samples are much lower than those for Co-rich. An interesting behavior is observed near room temperature where the power factor of several samples seems to increase with decreasing temperature. Low temperature measurements would be of interest and would clarify if this behavior is reproducible and provide information about the origin of this increase (if real). The power factor are maximum at about 200°C and a maximum value of $21 \ \mu W.cm^{-1}K^{-2}$ was achieved at this temperature.

Significant improvements in the figure of merit are possible by forming solid solutions only if the relative drop in lattice thermal conductivity is substantially larger than the drop in carrier mobility. The thermal diffusivity and heat capacity of several Co and Ir-rich solid solution samples was measured from room temperature up to about 500°C. These data were used to calculate the thermal conductivity of these samples and the results are shown in Figure 21. The results show that a very large drop in thermal conductivity was achieved compared to the values for $CoSb_3$ and $IrSb_3$ also shown in Figure 21. The sample doped with Tl shows a lower thermal conductivity than the other samples. This particularly low value might be related to a stronger mass disorder introduced by heavy Tl atoms in the lattice. However, more data would be needed on Tl doped samples to clarify this result. For all other samples, the thermal conductivity is nearly constant with temperature (typical of solid solution with strong point defect scattering) with a value of about 30 $W.m^{-1} \ K^{-1}$.

The figure of merit ZT was calculated for several samples and the results are shown in Figure 22. For all samples, the figure of merit is maximum around 300°C, increasing form room temperature and decreasing above this temperature. Although the thermal conductivity of the Tl doped sample was substantially lower than for the other samples, its power factor was also lower resulting in similar ZT values. A maximum value of 0.36 was measured on two samples. This represents a 160% improvement compared to the maximum value obtained for $IrSb_3$ (0.15). The reduction in carrier mobility in Co-rich solid solutions was substantially lower than the large reduction in thermal conductivity. Although large improvements in the figure of merit were obtained for n-type Co-rich $CoSb_3$-$IrSb_3$ solid solutions, the maximum ZT obtained are still relatively low and don't exceed the values of state of the art thermoelectric materials.

17

5. Conclusions

N-type samples of IrSb$_3$ were prepared using a liquid-solid phase sintering and also by hot-pressing of pre-reacted powders. Pt was found to be a good n-type dopant for IrSb$_3$. N-type samples have large Seebeck coefficients but higher electrical resistivity than p-type samples. High temperature transport property measurements showed that ZT values for n-type IrSb$_3$ are limited by relatively high thermal conductivity values: about 95 mW.cm^{-1}.K^{-1} at room temperature. N-type CoSb$_3$ crystals were grown using the gradient freeze technique and Te as a dopant. Similarly to IrSb$_3$, CoSb$_3$ samples have large Seebeck coefficients and higher electrical resistivity than p-type samples. ZT values for CoSb$_3$ are also limited by relatively high thermal conductivity values, about 95 mW.cm^{-1}.K^{-1} at room temperature.

Samples of one Ir-rich solid solution (Co$_{0.12}$Ir$_{0.88}$Sb$_3$) and two Co-rich solid solutions (Co$_{0.94}$Ir$_{0.06}$Sb$_3$ and Co$_{0.88}$Ir$_{0.12}$Sb$_3$) were prepared by the LSPS technique in order to investigate the decrease in lattice thermal conductivity due to increased point defect scattering. The dopants used were Pt for the Ir-rich solid solution Co$_{0.12}$Ir$_{0.88}$Sb$_3$, Pt and Te for Co-rich solid solution Co$_{0.94}$Ir$_{0.06}$Sb$_3$ and Pt, Tl, In and Te for the Co-rich solid solution Co$_{0.88}$Ir$_{0.12}$Sb$_3$. High temperature measurements showed that a substantial decrease in thermal conductivity was obtained and the typical value obtained at room temperature is about 30 mW.cm^{-1}.K^{-1}, a reduction of about 70% compared to the binary compounds. It also been found that the Seebeck coefficient values are similar for Co and Ir-rich solid solution samples but the Hall mobility values of Ir-rich solid solution samples are substantially lower than those for Co-rich solid solution samples, resulting in higher electrical resistivity values. Hence, the power factor values for Co-rich solid solutions are much larger than those for the Ir-rich solid solution. A maximum ZT of about 0.36 was measured on Co-rich solid solution samples which represents a 160% improvement compared to ZT values measured for the binary compounds.

6. References

1. T. Caillat, A. Borshchevsky and J.-P. Fleurial, "Novel Transition Metal Compounds with Promising Thermoelectric Properties", *Proceedings of the XIIth International Conference on Thermoelectrics,* 1 132-136, Yokohama, Japan, November 9-11 (1993).

2. Oftedal, I., *Z. Kristallogr.*, 66, 517 (1928).

3. A. Kjekshus, D. G. Nicholson, T. Rakke, *Acta Chem. Scand.*, 27, 4 (1973).

4. T. Caillat, A. Borshchevsky, J. P. Fleurial, in K. R. Rao (ed.), *Proc. 11th Int. Conf. on Thermoelectrics,* Arlington, TX, The University of Texas, Arlington, 98 (1993).

5. G. Kliche, W. Bauhofer, *Mat. Res. Bull.*, 22, 551 (1987).

6. J. P. Odile, S. Soled, C. A. Castro, A. Wold, *Inorganic Chemistry,* 17, 2, 283 (1978).

7. F. Hulliger, *Helv. Phys. Acta*, 34, 782 (1961).

8. N. Mandel, J. Donohue, *Acta Cryst.*, B27, 2288 (1971).

9. C. M. Pleass, R. D. Heyding, *Canadian Journal of Chemistry*, 40, 590 (1962).

10. H. D. Lutz, G. Kliche, *Journal of Solid State Chemistry*, 40, 64 (1981).

11. T. Caillat, A. Borshchevsky and J.-P. Fleurial, "Phase Diagram of the Ir-Sb System on the Antimony-Rich Part", Journal of Alloys and Compounds, <u>199</u>, 207-210 (1993).

12. J.A. McCormack and J.P. Fleurial, "Electrical Characterization of SiGe Thin Films", in *Modern Perspectives on Thermoelectrics and Related Materials*, MRS Symp. Proc. Vol. 234, 135-143, (Materials Research Society, Pittsburg, Pennsylvania 1991).

13. C. Wood, D. Zoltan and G. Stapfer "Measurement of Seebeck Coefficient Using a Light Pulse", Rev. Sci. Instrum. 56 (5), 719-722, 1985.

14. J.W. Vandersande, C. Wood, A. Zoltan and D. Whittenberger, *Thermal Conductivity 19*, Plenum Press, New York, 445-452 (1988).

15. T. Caillat, A. Borshchevsky and J.-P. Fleurial, "Preparation and Thermoelectric Properties of p and n-Type IrSb$_3$", ", *Presented at the XIIIth International Conference on Thermoelectrics*, Kansas City, 1994

16. *Binary Alloy Phase Diagrams*, 2nd ed., T. Massalski, Ed., (1990).

17. T. Caillat, A. Borshchevsky and J.-P. Fleurial, "Preparation and Thermoelectric Properties of p and n-Type CoSb$_3$", ", *Presented at the XIIIth International Conference on Thermoelectrics*, Kansas City, 1994

18. A. Borshchevsky, E. Allevato, J.-P. Fleurial and T. Caillat, "CoSb$_3$-IrSb$_3$ Solid Solutions: Preparation and Characterization", ", *Presented at the XIIIth International Conference on Thermoelectrics*, Kansas City, 1994.
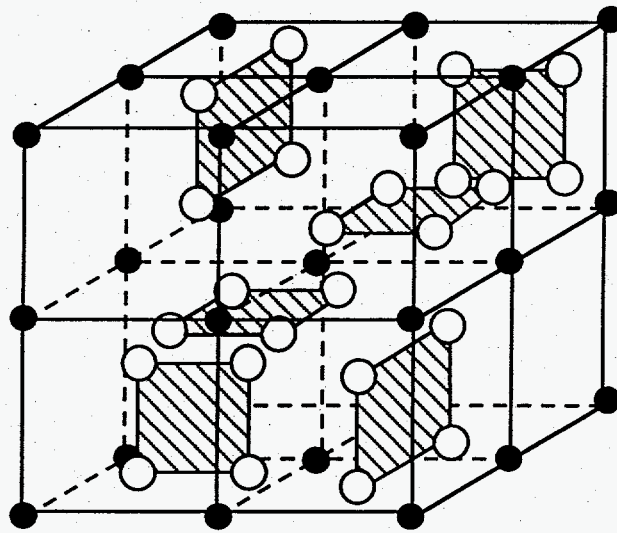
● T: transition metal

○ Pn: pnicogen

Figure 1: Skutterudite Unit Cell
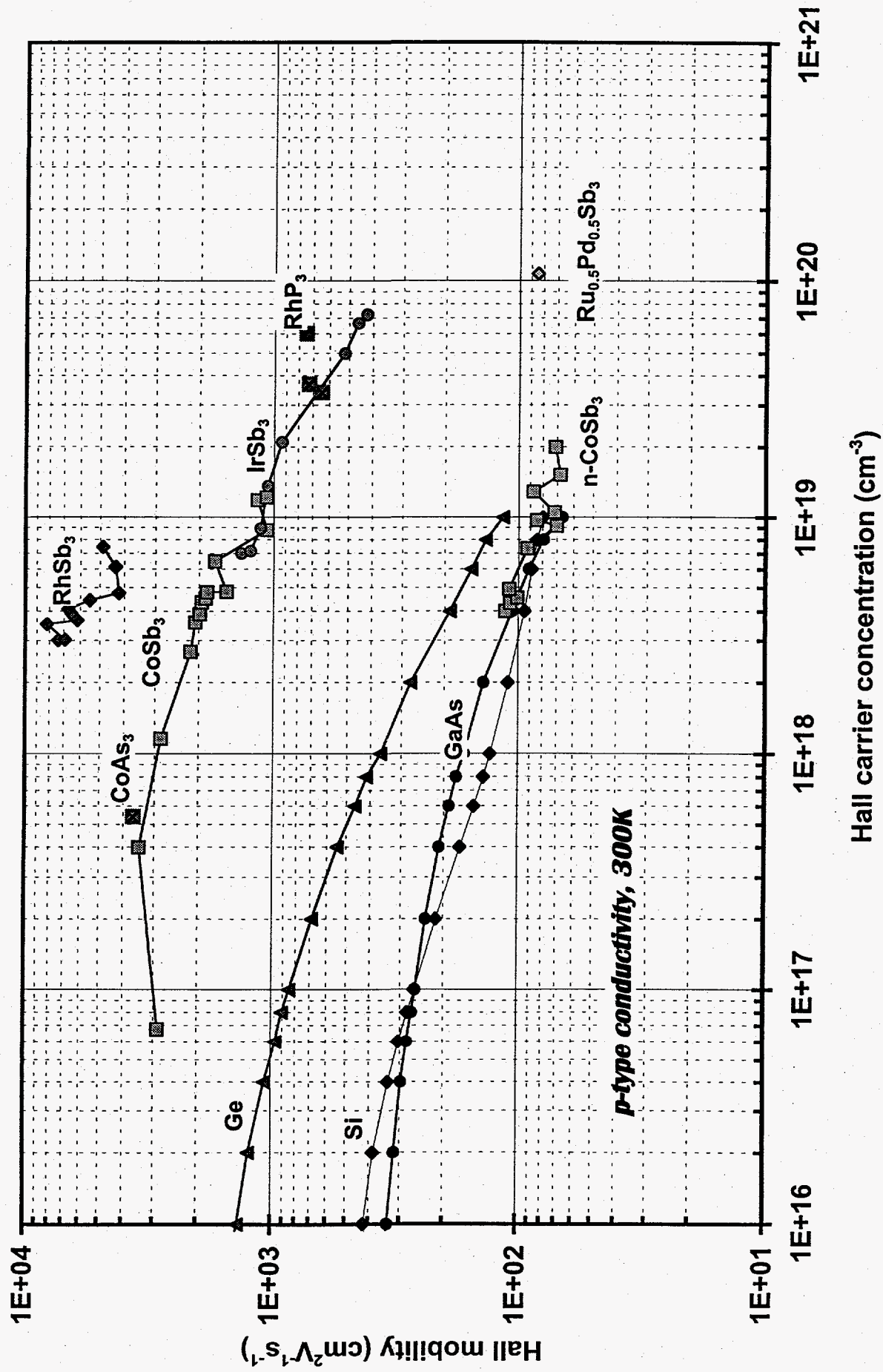
Figure 2: Room temperature Hall mobility as a function of carrier concentration of skutterudites and comparison with state of the art semiconductors
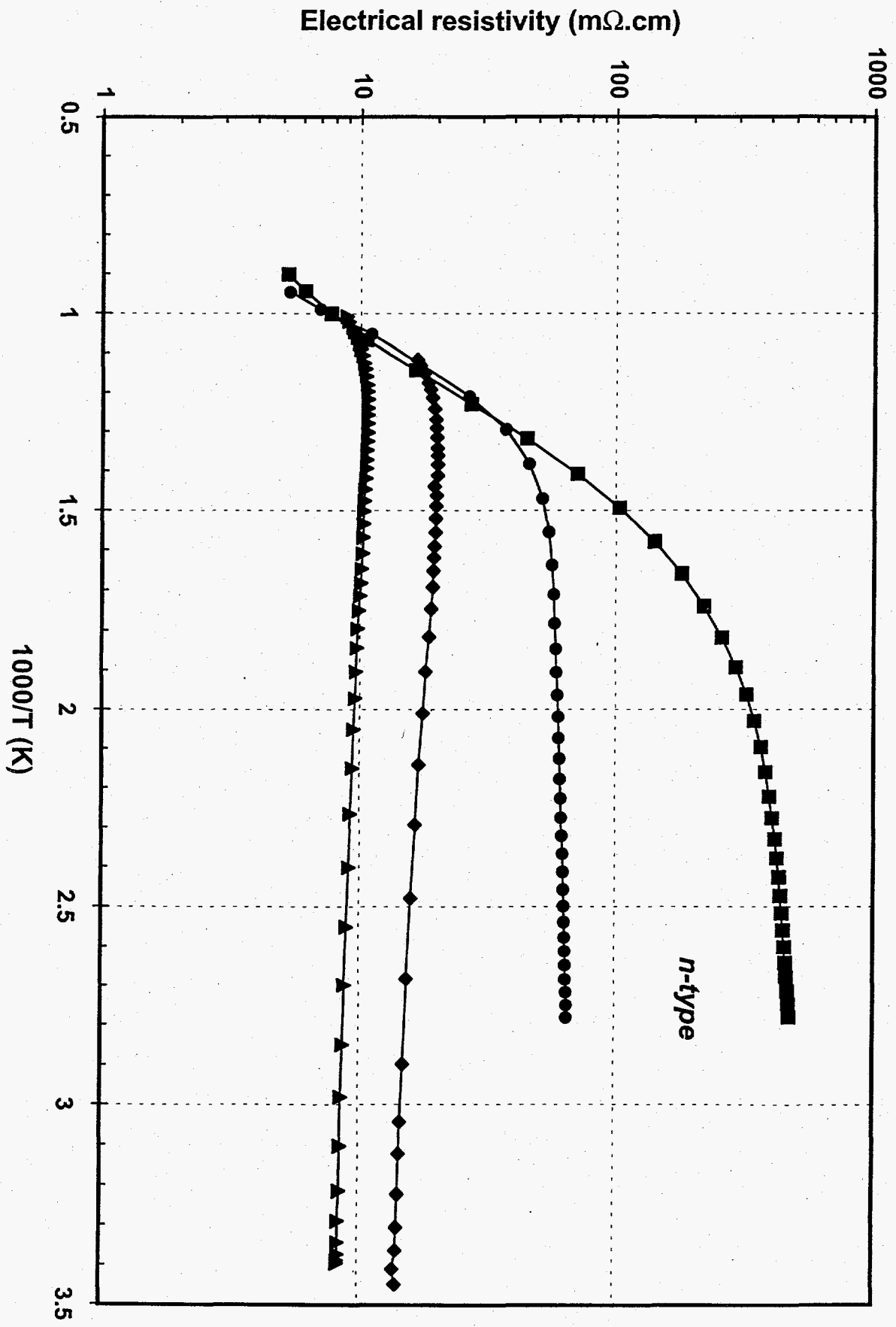
Figure 3: Electrical resistivity as a function of inverse temperature for n-type IrSb3
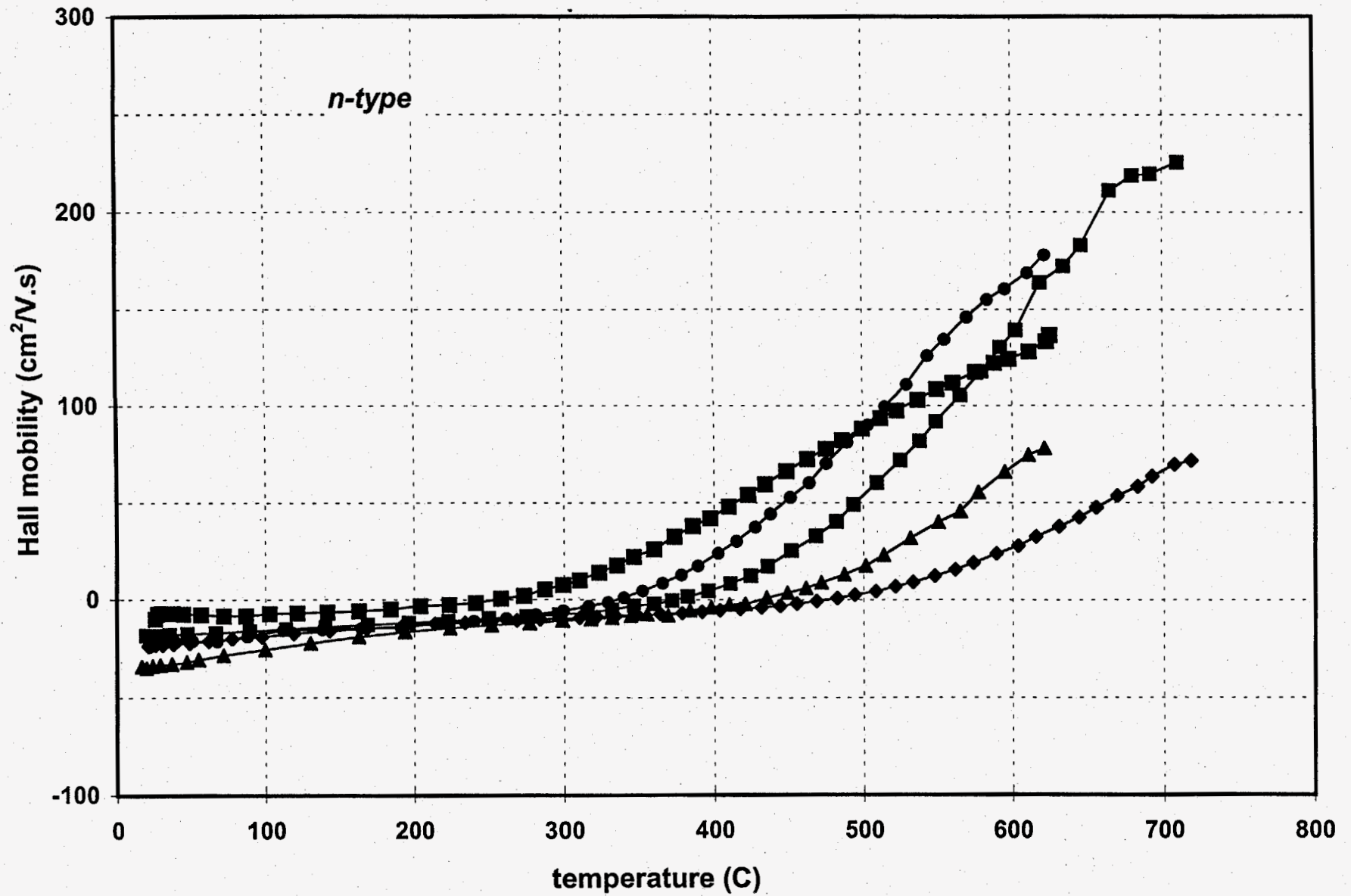
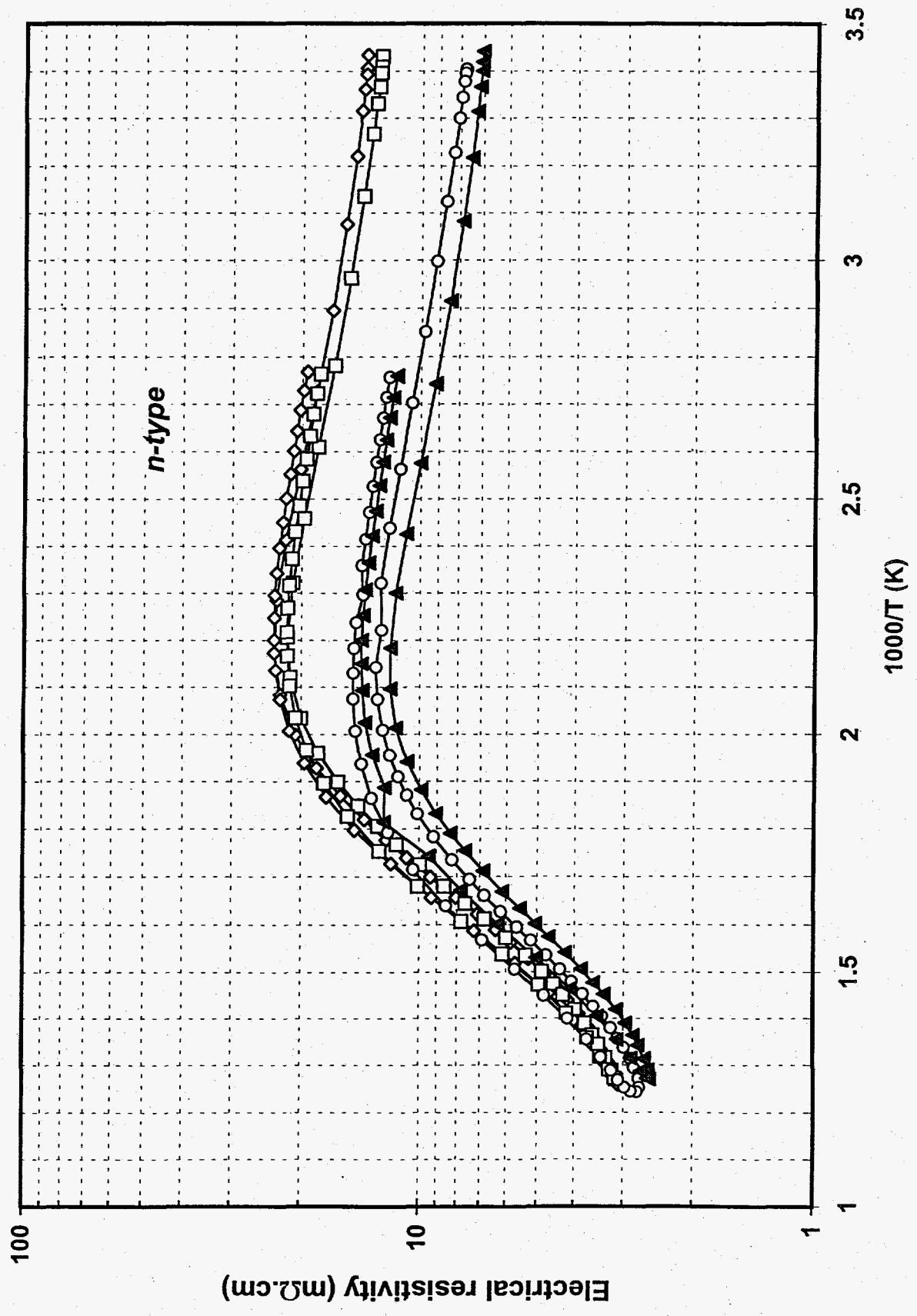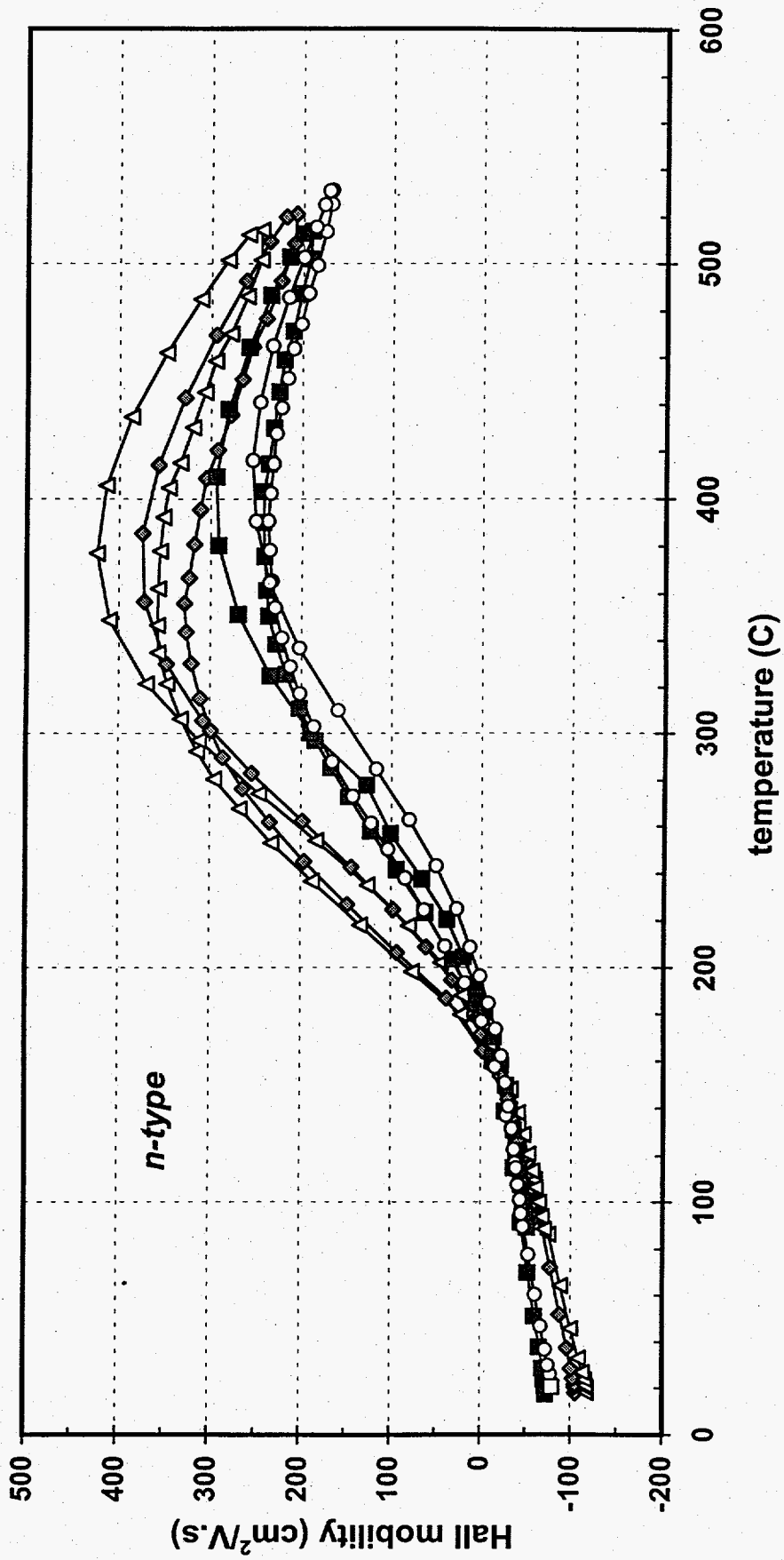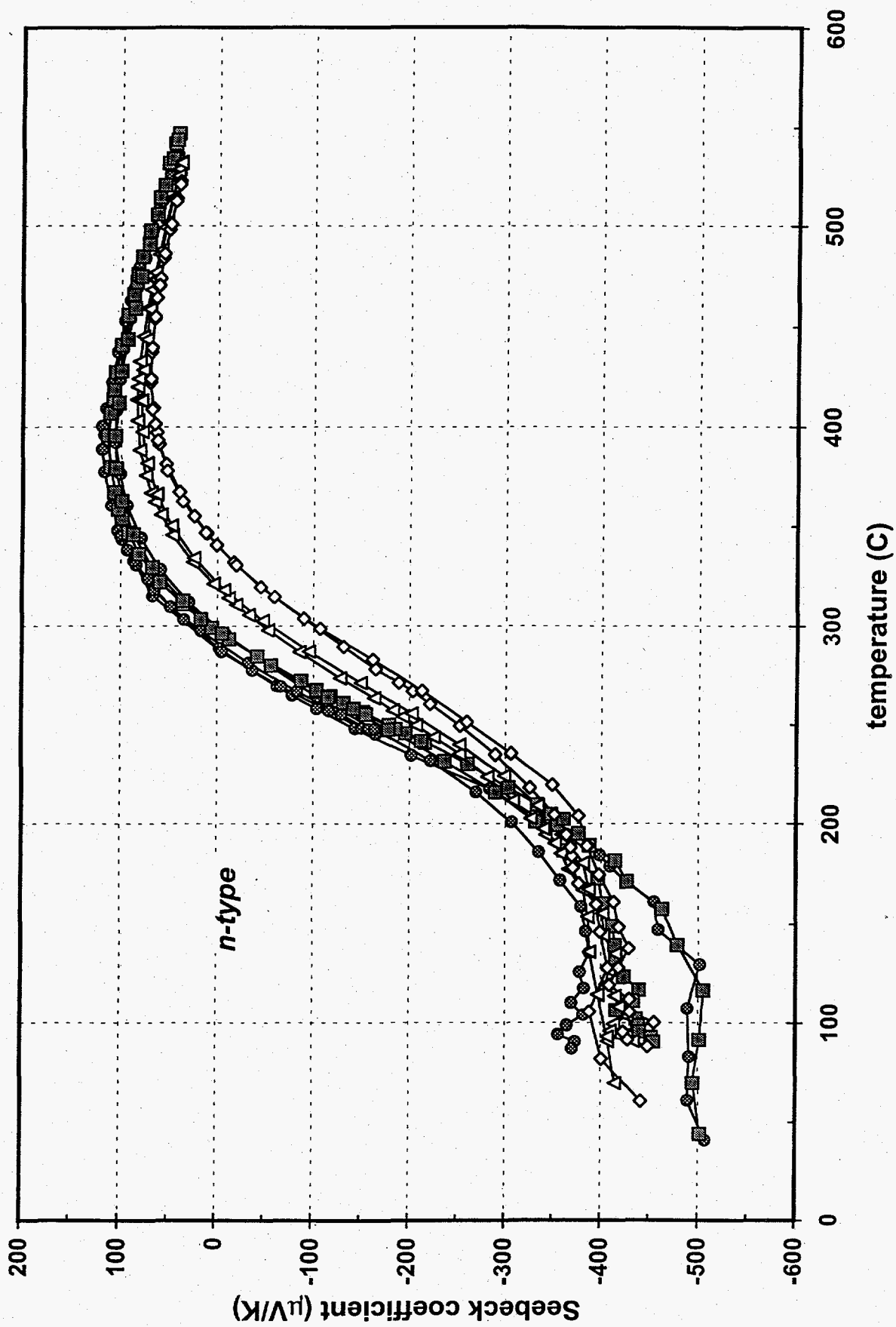**Figure 4**: Hall mobility as a function of temperature for n-type IrSb3
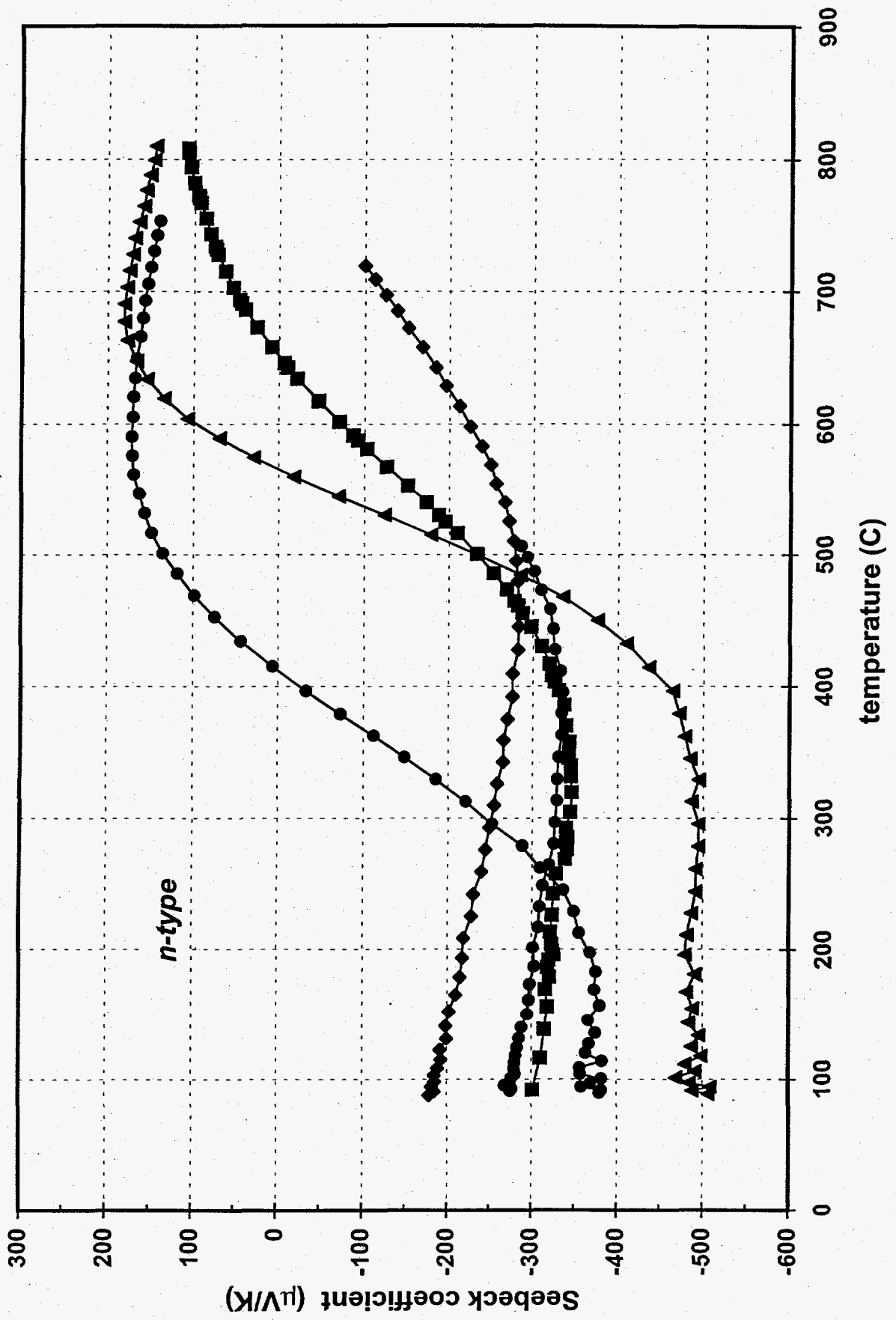
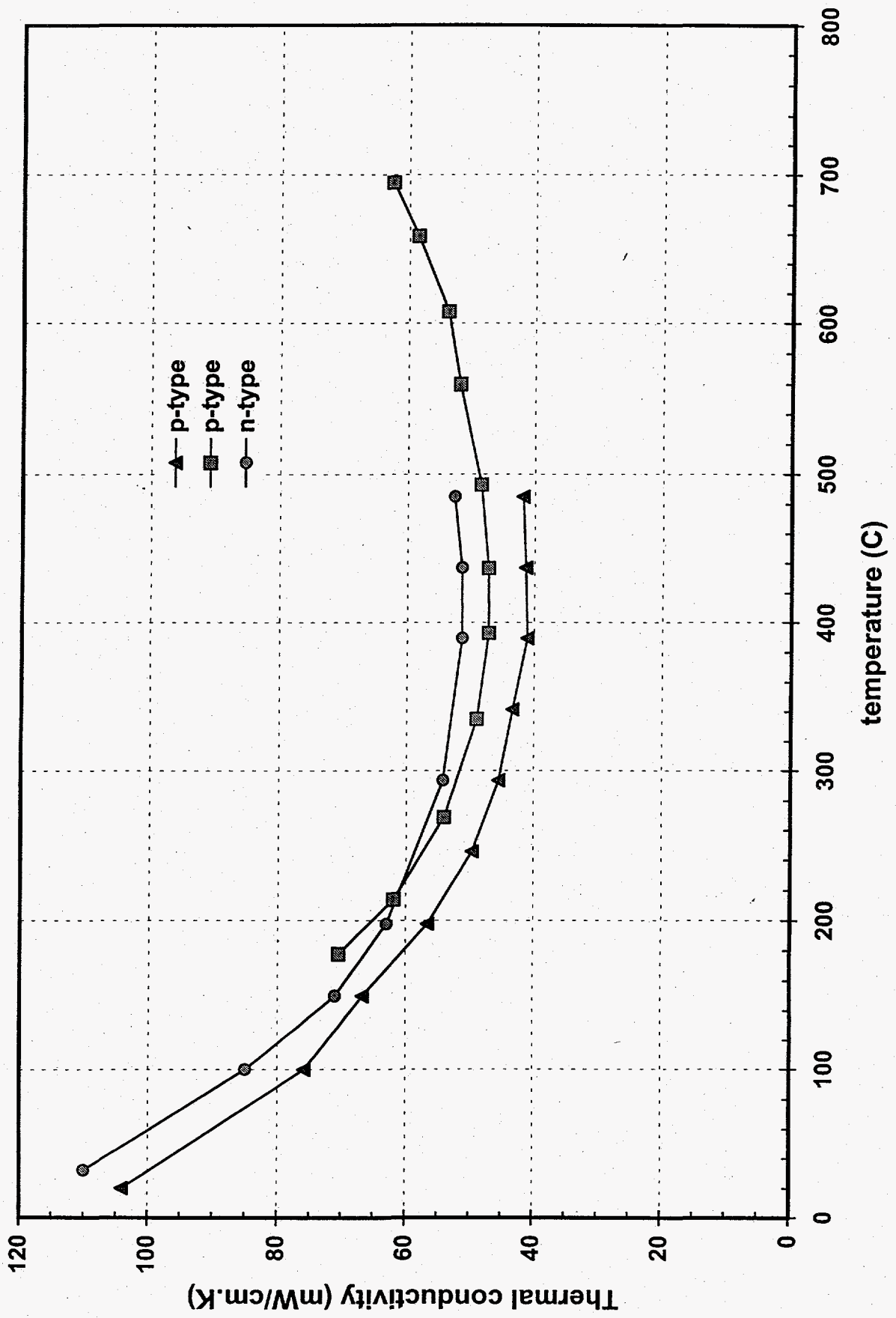**Figure 5: Seebeck coefficient as a function of temperature for n-type IrSb3**
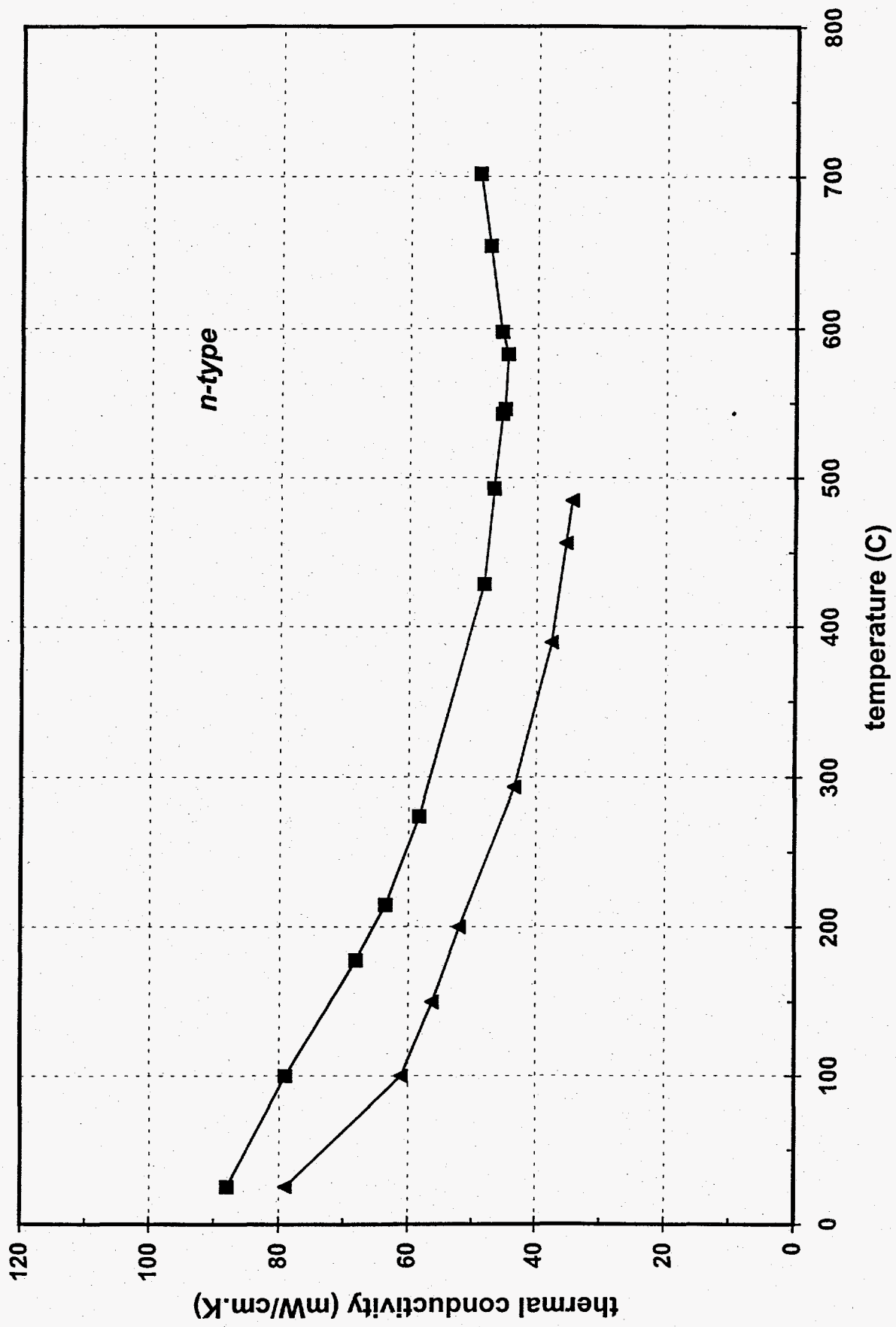
Figure 6: Thermal conductivity as a function of temperature for n-type Irsb3
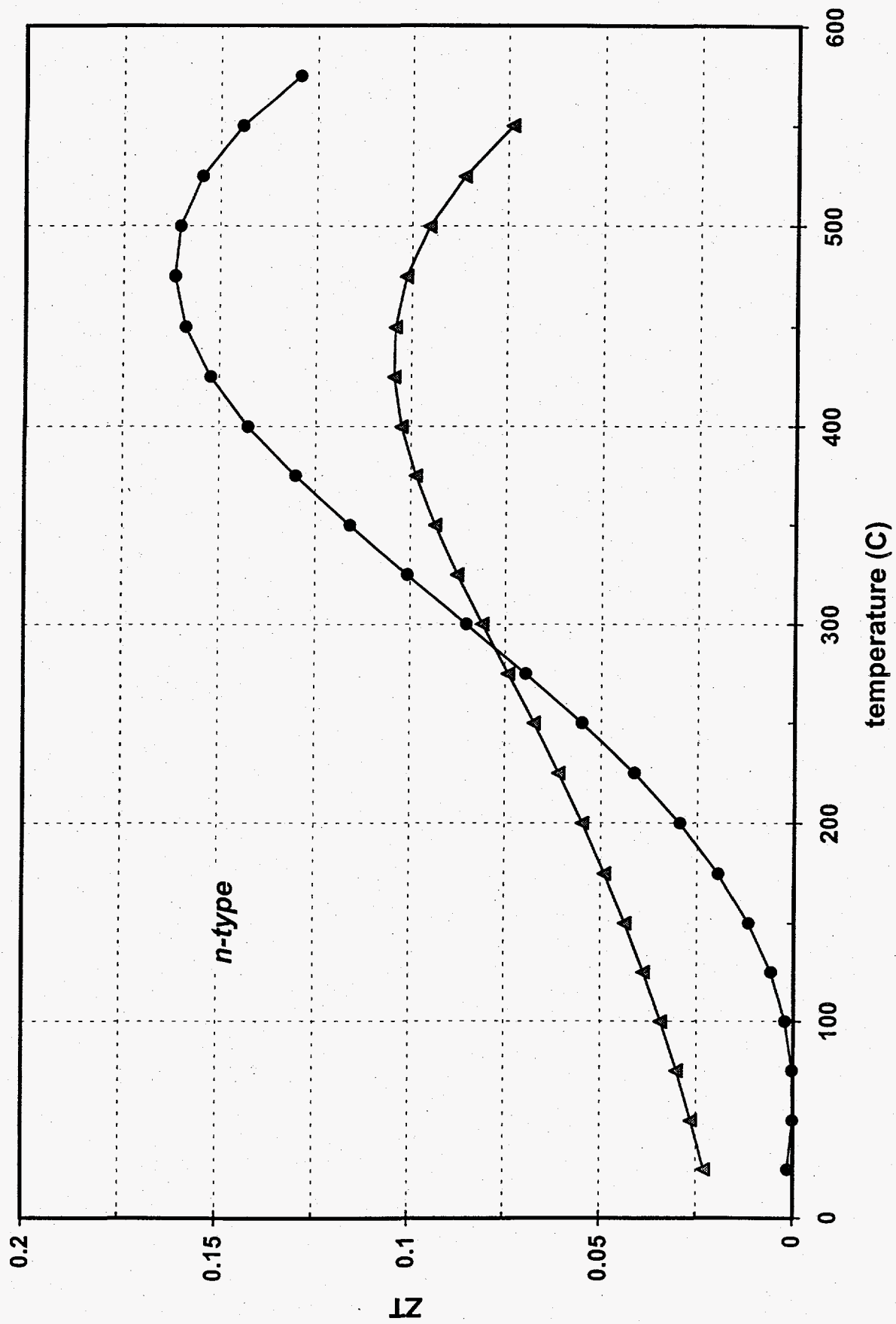
Figure 7: Dimensionless figure of merit ZT as a function of temperature for n-type IrSb3

Figure 8: Electrical resistivity as a function of inverse temperature for n-type CoSb3

Figure 9: Hall mobility as a function of temperature for n-type CoSb3

Figure 10: Seebeck coefficient as a function of temperature for n-type CoSb3

Figure 11: Thermal conductivity as a function of temperature for n- and p-type CoSb3
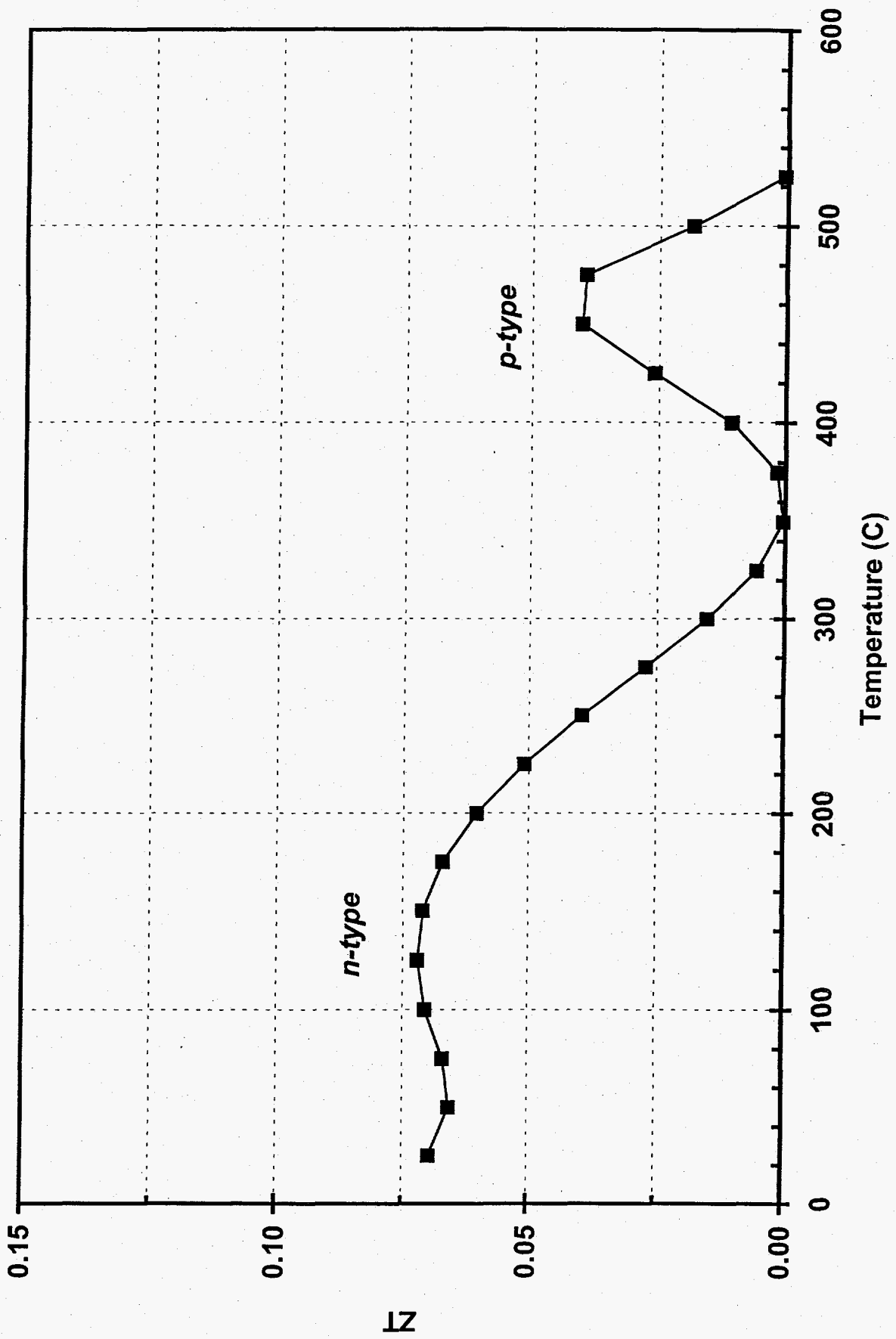
Figure 12: Dimensionless figure of merit ZT as a function of temperature for n-type CoSb3
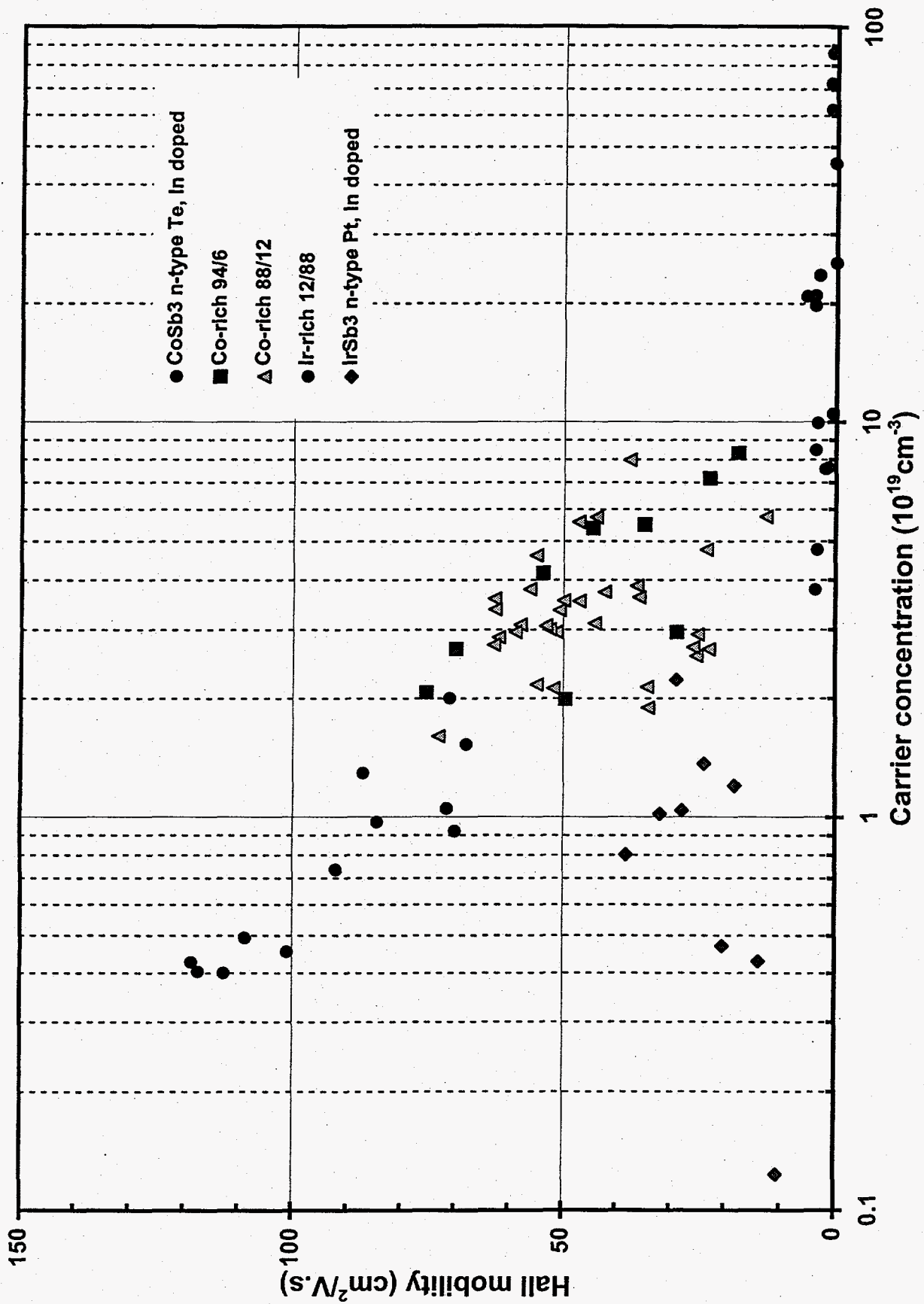
Figure 13: Room temperature Hall mobility as a function of carrier concentration for n-type CoSb3, IrSb3 and several CoxIr1-xSb3 solid solutions
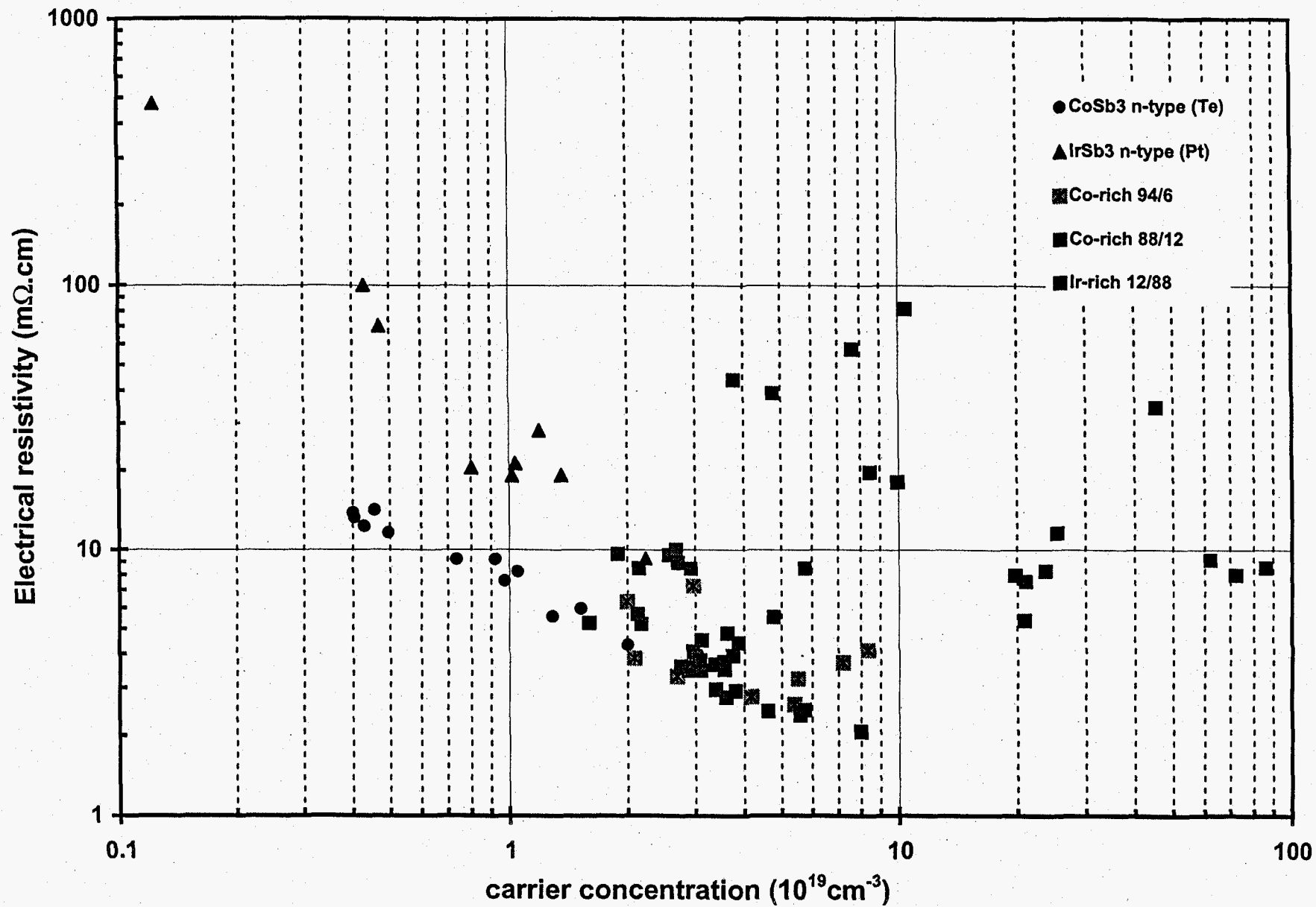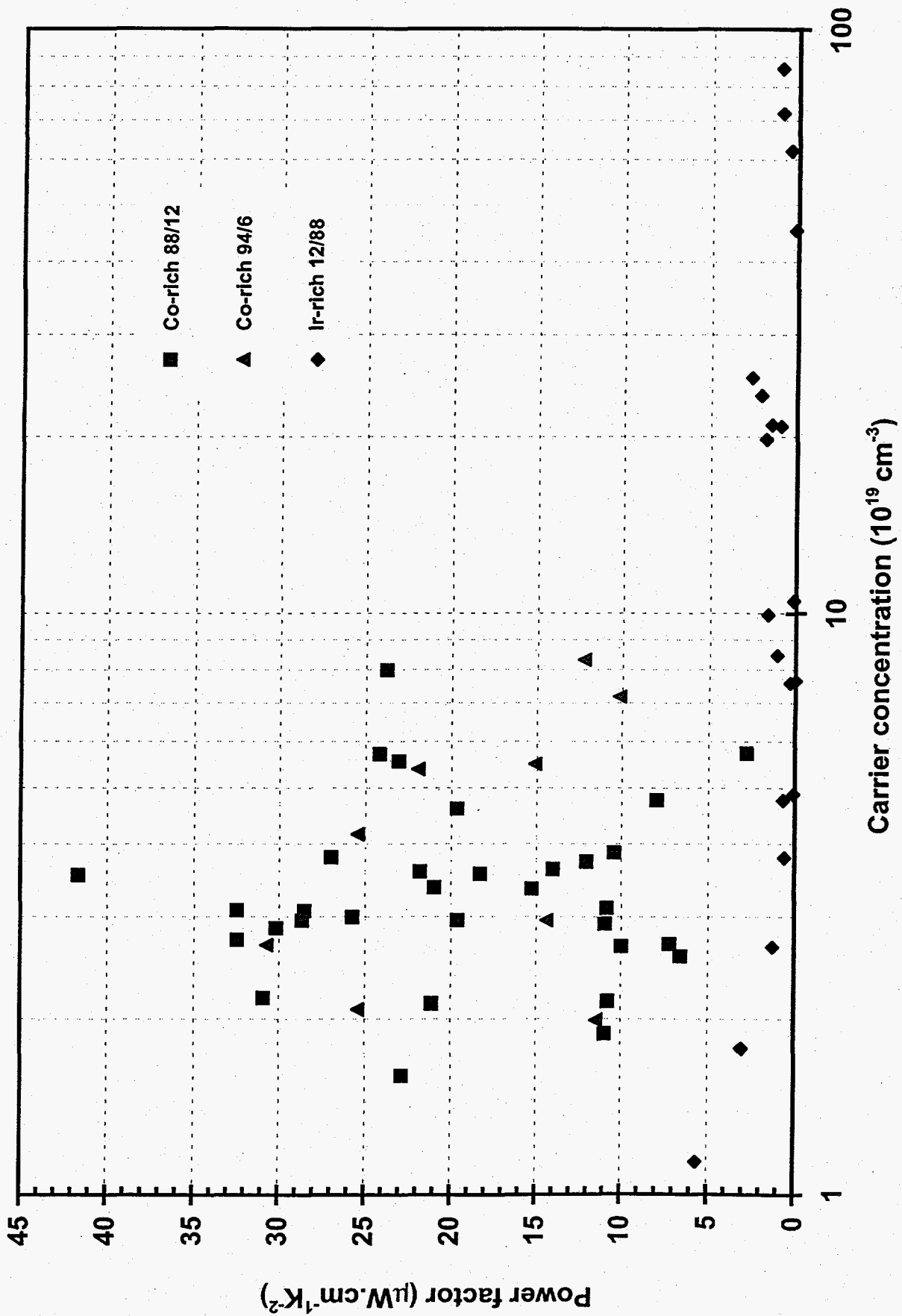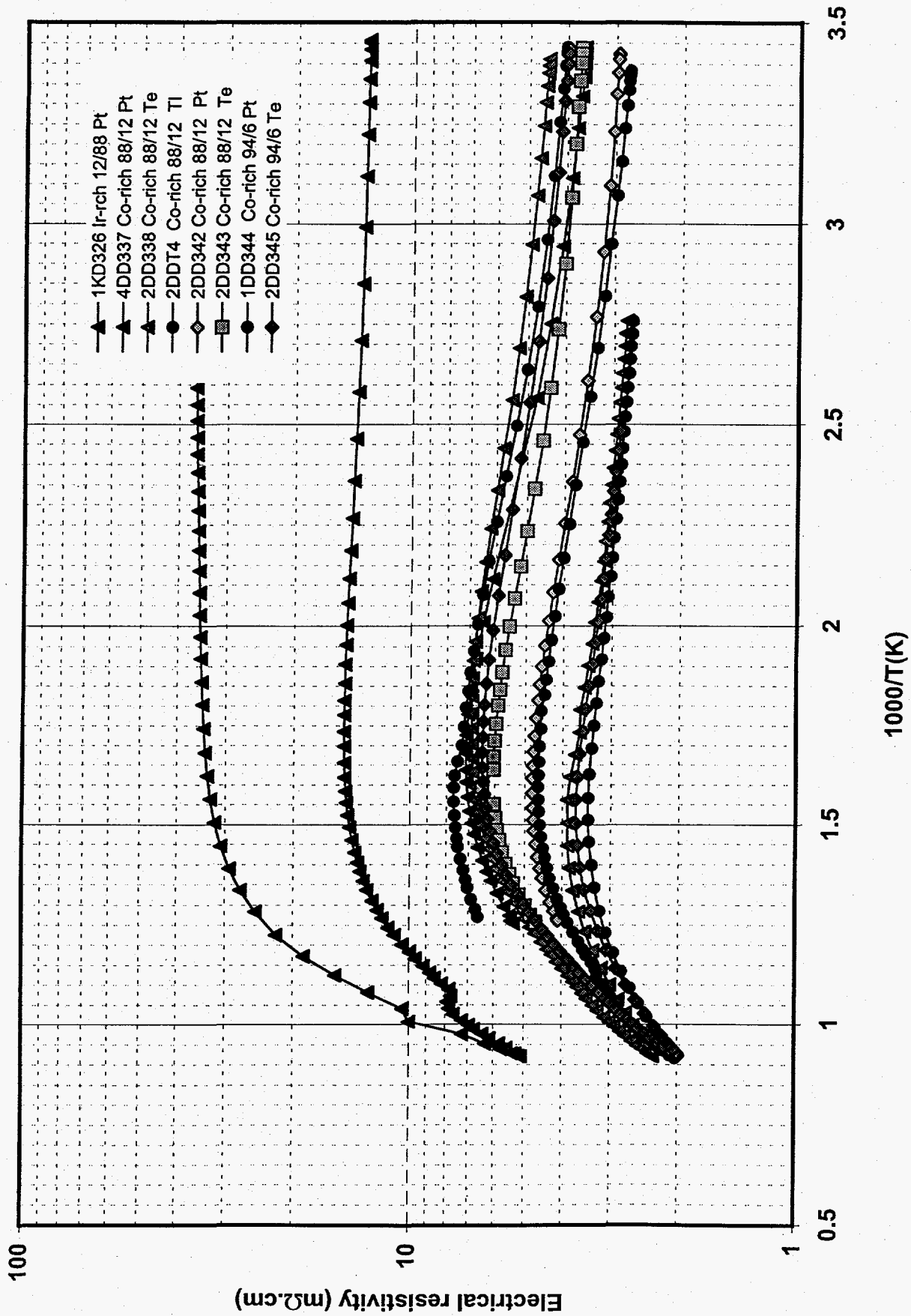
Figure 14: Room temperature electrical resistivity as a function of carrier concentration for n-type CoSb3, IrSb3 and several CoxIr1-xSb3 solid solutions
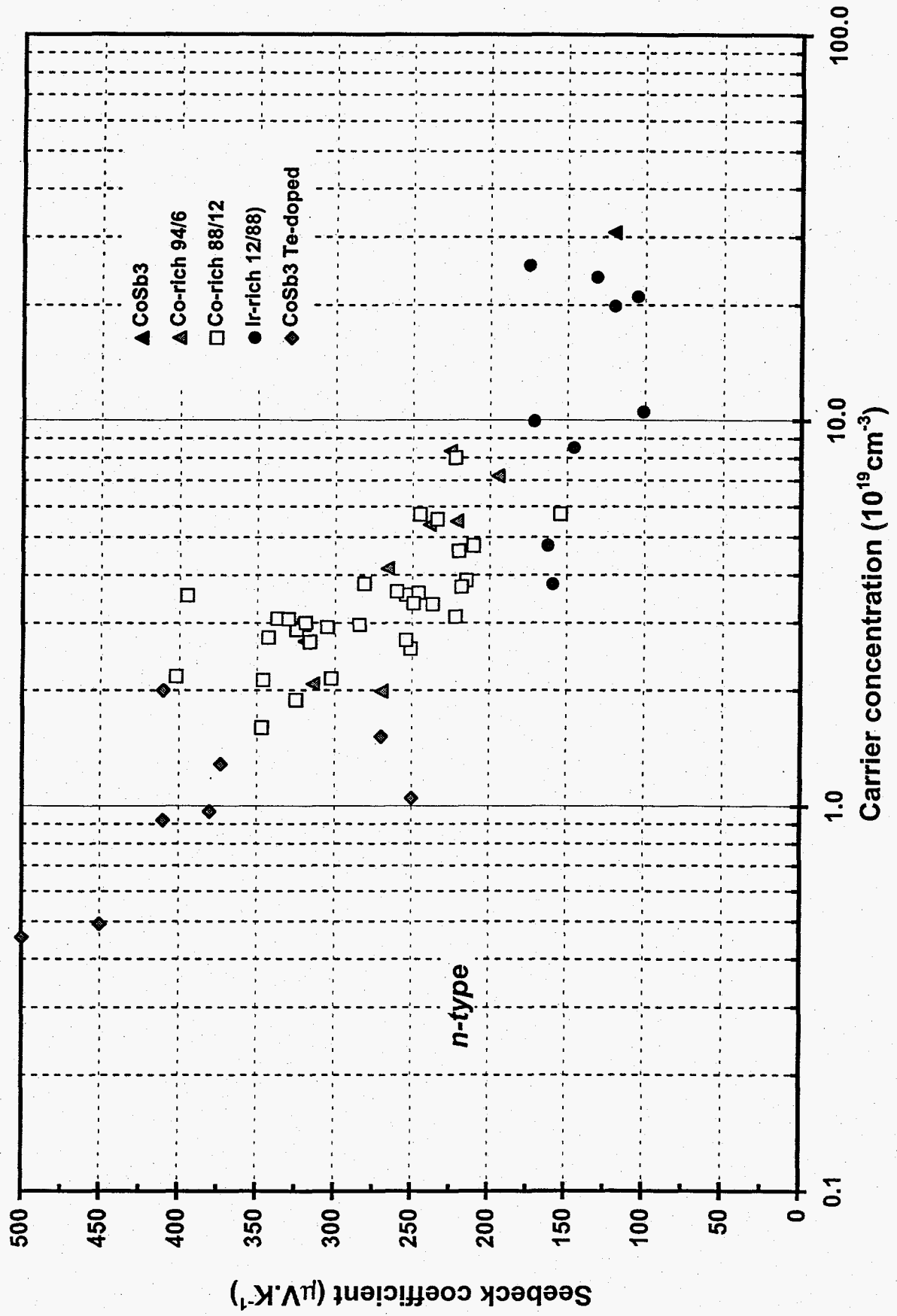
Figure 15: Room temperature Seebeck coefficient as a function of carrier concentration for n-type CoSb3, IrSb3 and several CoxIr1-xSb3 solid solutions

Figure 16: Room temperature power factor as a function of carrier concentration for several $Co_xSb1-xSb3$ n-type solid solutions

Legend:
- 1KD326 Ir-rch 12/88 Pt
- 4DD337 Co-rich 88/12 Pt
- 2DD338 Co-rich 88/12 Te
- 2DDT4 Co-rich 88/12 Tl
- 2DD342 Co-rich 88/12 Pt
- 2DD343 Co-rich 88/12 Te
- 1DD344 Co-rich 94/6 Pt
- 2DD345 Co-rich 94/6 Te

Electrical resistivity (mΩ.cm)

1000/T(K)

Figure 17: Electrical resistivity as a function of inverse temperature for n-type CoSb3-IrSb3 solid solutions
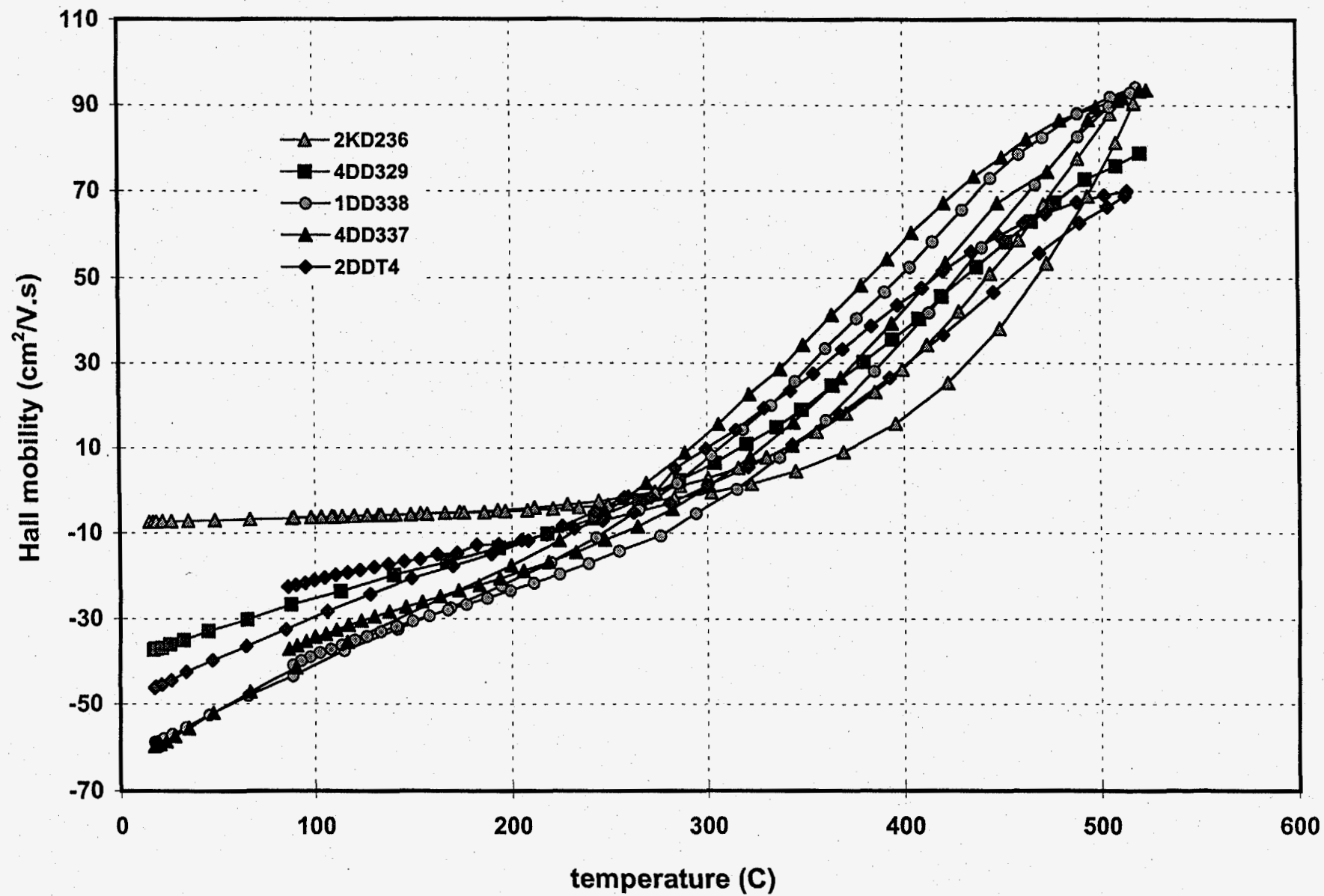
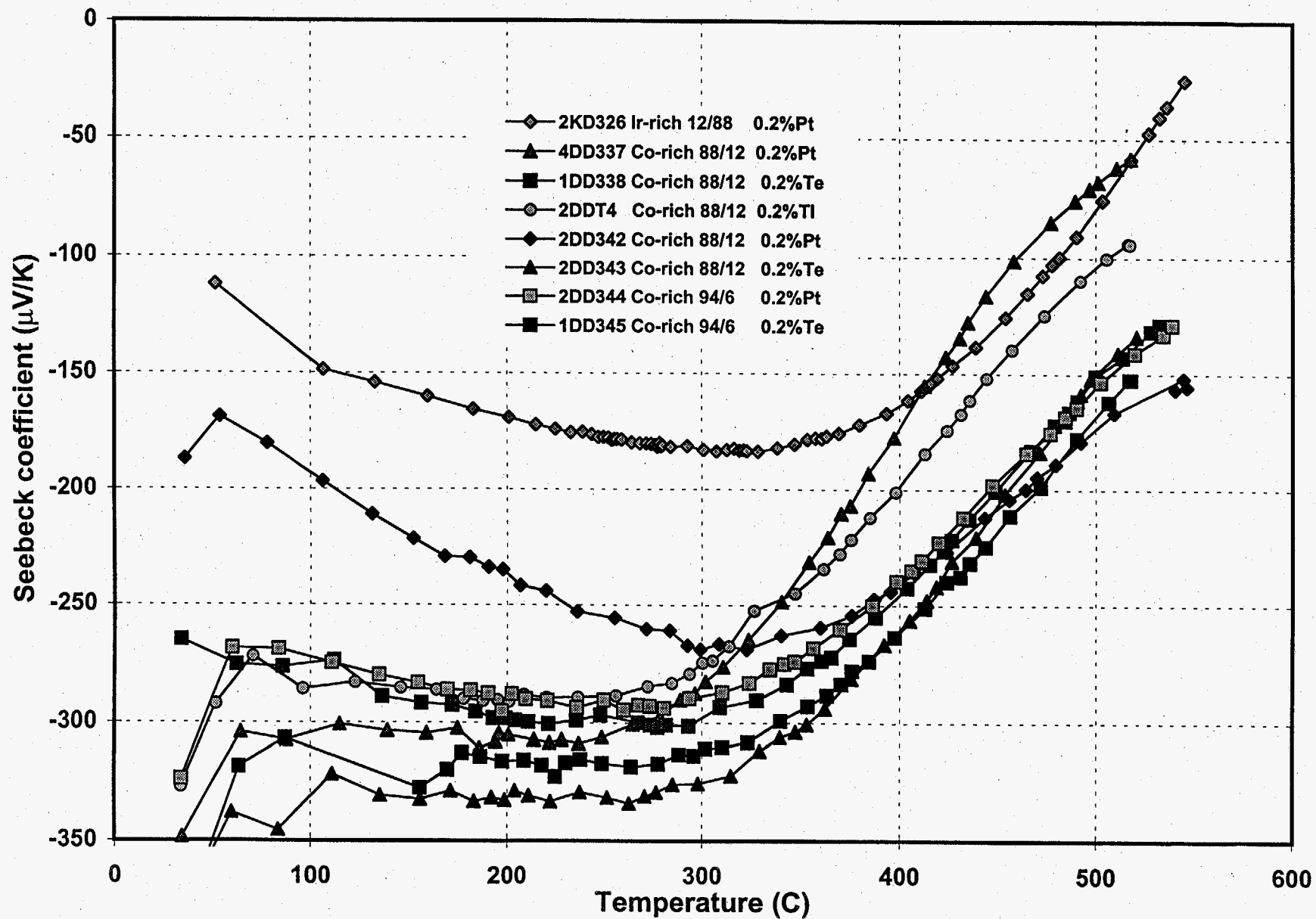**Figure 18**: Hall mobility as a function of temperature for n-type Cosb3-IrSb3 solid soltuions

Figure 19: Seebeck coefficient as a function of temperature for several n-type CoSb3-IrSb3 solid solutions
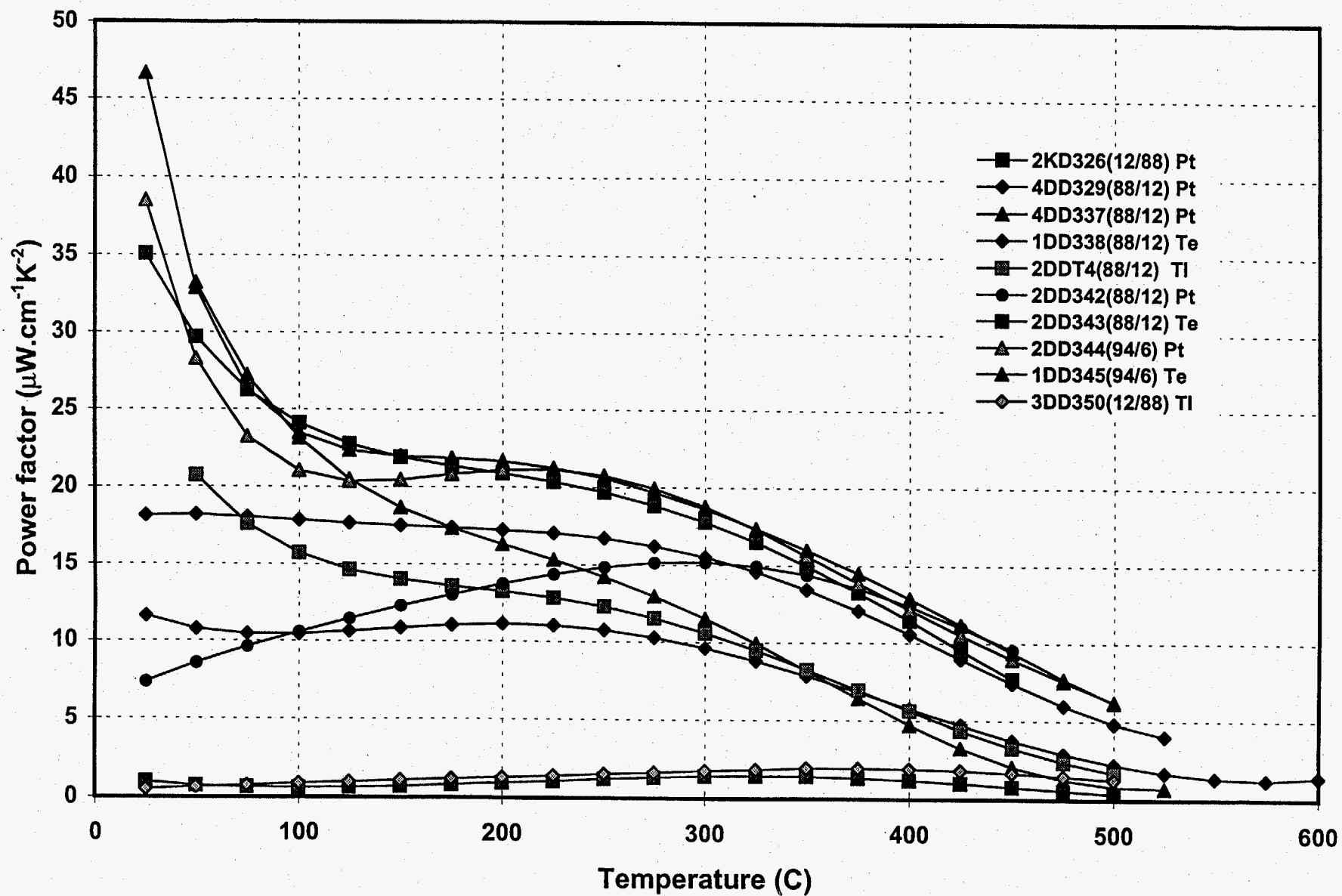
<u>Figure 20</u>: Power factor as a function of temperature for n-type CoSb3-IrSb3 solid solutions
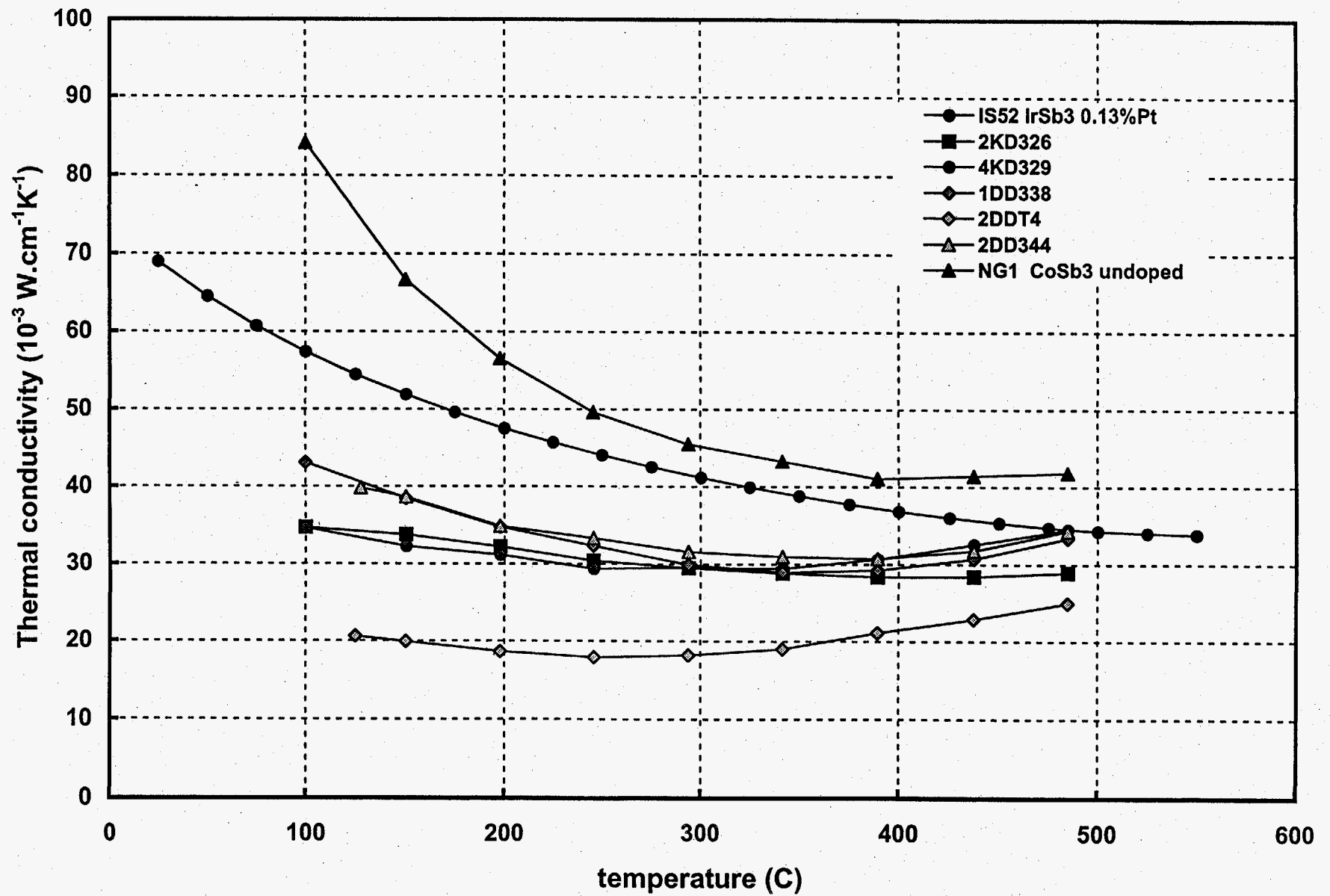
Figure 21: Thermal conductivity as a function of temperature for n-type Cosb3-Irsb3 solid solutions
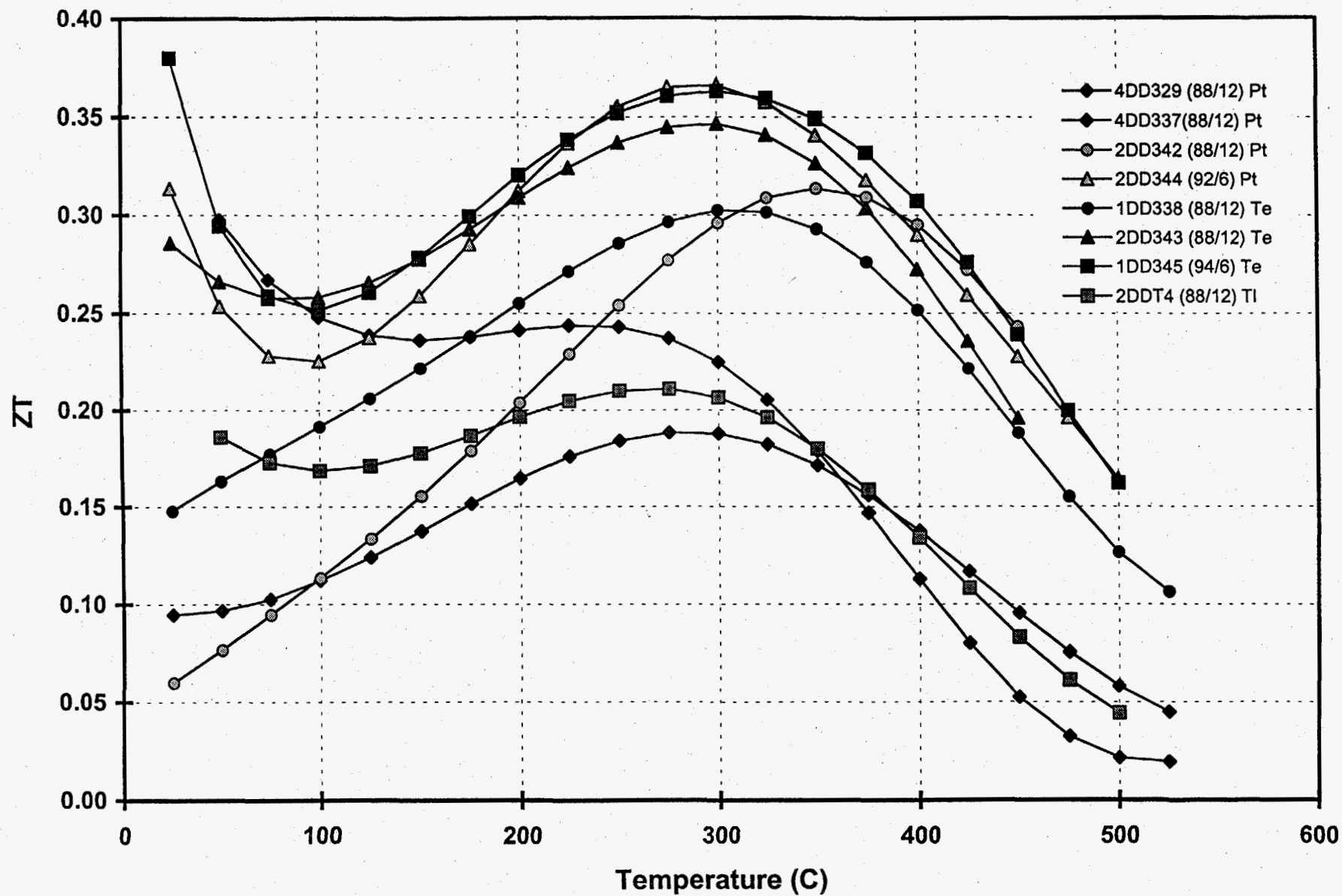
Figure 22: ZT as a function of temperature for n-type CoSb3-IrSb3 solid solutions